Higher meiotic chromosome condensation: a potential function of kinetochore through polo-like kinase

Authors: Deepika Trakroo, Prakhar Agarwal[#], Anushka Alekar[#], and Santanu Kumar Ghosh*

Affiliation: Department of Biosciences and Bioengineering, Indian Institute of Technology, Bombay, Powai, Mumbai-400076, India.

# Equal contribution

*Corresponding author

Email: santanughosh@iitb.ac.in

Tel. +(91-22) 2576 7766

Key words: Meiosis, chromosome, kinetochore, condensin, budding yeast

Abstract

Chromosome condensation plays a pivotal role during faithful chromosome segregation, hence understanding the factors that drive condensation is crucial to get mechanistic insight into chromosome segregation. The results of our in vivo chromosome condensation assays in budding yeast reveal that chromosomes undergo a higher degree of condensation during meiosis than in mitosis. Earlier the non-essential kinetochore proteins were shown to have several significant meiotic functions. We conclude that these proteins might also have a role in achieving higher meiotic condensation since we observed meiotic-specific condensation defects in the absence of the non-essential kinetochore protein, Ctf19. While investigating the mechanism involved, we observed an accumulation of the polo-like kinase Cdc5 owing to its higher protein stability in *ctf19Δ* meiotic cells. High Cdc5 activity leads to hyper-phosphorylation of the condensin which shows reduced stability with concomitant decreased association with the chromatin. Overall, our findings highlight the role of Ctf19 in promoting meiotic chromosome condensation by influencing the activity of Cdc5 and thereby affecting the stability and association of condensin with the chromatin.

Introduction

Faithful chromosome segregation across eukaryotes requires that the chromosomes become condensed and attached properly to the microtubule spindle during cell division. The attachment is mediated by a conserved multiprotein complex called 'kinetochore' formed at the centromeres of the chromosomes (Schrader,1939). The proteins within a kinetochore are organized in a hierarchical fashion with respect to the centromeric DNA and the microtubules. The inner and the outer proteins associate with the centromeres and microtubules, respectively whereas the central

43 proteins act as linker (Meraldi et al., 2006, Dong et al., 2022, Dou et al., 2023). Over the last three
44 decades studies on kinetochore from myriad organisms have revealed that this protein complex,
45 besides establishing a connection with the microtubules, also controls other cellular activities that
46 facilitate high-fidelity chromosome segregation. For instance, the promotion of pericentric
47 enrichment of cohesin complex that keeps the sister chromatids together from the S phase till
48 anaphase (Glynn et al., 2004, Eckert et al. 2007, Holt et al., 2005, Fernius et al., 2013), early
49 replication of the centromeres that ensures correct deposition of the centromeric histone 3 variant
50 (Raghuraman et al., 2001, Muller et al., 2012, Natsume et al., 2013), late assembly of the
51 kinetochore in meiosis to facilitate co-orientation of the sister kinetochores during meiosis I
52 (Meyer et al., 2015) and homolog pairing in meiosis by causing 'centromere coupling' (Tsubouchi
53 et al., 2005, Kim et al., 2013).

54 In budding and fission yeasts, the kinetochore proteins, in particular the essential inner and
55 central proteins, are also shown to promote chromosome condensation (Kruitwagen et al., 2018,
56 Nakazawa et al., 2008). Subsequent studies revealed that this happens through kinetochore-
57 mediated centromeric and pericentromeric recruitment of several proteins including cohesins
58 (Guacci et al., 1997, Lavoie et al., 2004), shugoshin (Peplowska et al., 2014, Kruitwagen et al.,
59 2018, Yahya et al., 2020), 14-3-3 protein, Bmh1 (Jain et al., 2021) and enzymes such as aurora B
60 kinase, Ipl1 (Giet et al., 2001, Petersen et al., 2003, Lavoie et al., 2004,), polo-like kinase, Cdc5
61 (St. Pierre et al., 2009, Bazile et al., 2010, Leonard et al., 2015, Lamothe et al., 2020,) and a
62 histone deacetylase, Hst2 (Wilkins et al., 2014, Kruitwagen et al., 2015, 2018, Jain et al., 2021).
63 However, the non-essential proteins of the Ctf19 sub-complex (Ctf19c) of the kinetochore (Mehta
64 et al., 2022) were not shown to hinder chromosome condensation (Kruitwagen et al., 2018) as
65 expected from their dispensability in mitotic growth. However, we have shown earlier that in
66 absence of these non-essential proteins, meiosis is severely affected as several meiosis specific

events are perturbed (Ghosh et al., 2004, Mehta et al., 2014, Agarwal et al., 2015). This happens as there appears to be a differential organization of the kinetochore assembly between mitosis and meiosis (Mehta et al., 2014, Borek et al., 2021) for which the non-essential proteins perhaps facilitate certain protein-protein and/or protein-DNA interactions in meiosis but not in mitosis.

Strikingly, earlier we observed that Ctf19 has a role to play in meiotic chromosome condensation since the cells in the absence of Ctf19 harbor defects in rDNA condensation and show reduced association of condensin with the chromatin in meiosis but not in mitosis (Mehta et al., 2014). While why chromatin-condensin association is compromised in *ctf19Δ* meiotic cells is not known, we hypothesize that to facilitate prophase I events, meiosis may require extra chromosome condensation than mitosis and the nonessential kinetochore proteins might contribute to regulating that. This notion is also fueled by the distinct thread-like appearance of the paired homologous chromosomes in pachytene of meiosis I which is never visible in mitosis and unlikely to happen in meiosis solely due to pairing.

In this report, to test the above hypothesis we sought to compare the extent of chromosome condensation between mitosis and meiosis and to find a molecular explanation of condensation defect in the non-essential kinetochore mutants. Interestingly, we observed using three cell biological in vivo assays that the chromosomes are indeed more condensed in meiosis than in mitosis. We further demonstrate that lack of Ctf19 causes misregulation of Cdc5 specifically in meiosis, which leads to hyper-phosphorylation of condensin resulting its dissociation from the chromatin and defect in chromosome condensation. Additionally, using wild type cells overexpressing Cdc5, we show that the misregulation of Cdc5 is indeed the reason for condensin failing to associate properly with the chromatin. This study highlights yet another meiosis-specific essential contribution of the mitotically dispensable kinetochore proteins.

90

91 **Results**

92 **Chromosomes are more condensed in meiosis as compared to mitosis**

93 We hypothesize that the level and determinants of chromosome condensation might differ between
94 mitosis and meiosis because earlier using Ctf19c mutant we observed that the kinetochore has a
95 role in rDNA condensation in meiosis but not in mitosis (Mehta et al., 2014). However, whether
96 such a role is confined to a specific condensed locus like rDNA or it is observed at other
97 chromosomal locales remains unknown. To investigate this, we first sought out to compare the
98 extent of chromosomal condensation of the kinetochore proximal pericentromeric regions between
99 mitosis and meiosis. Diploid strains were constructed where one copy of chromosome V was
100 marked with $[TetO]_{224}$ –[TetR-GFP] system at a locus 1.4 kb away from the *CEN V* (henceforth
101 called *CEN V*-GFP). The fluorescence intensity of *CEN V*-GFP was used as a surrogate marker to
102 decipher the in vivo condensation level as described before (Kruitwagen et al., 2015). In this
103 microscopy-based assay, the fluorescence intensity of TetR-GFP bound to the $[TetO]_n$ array
104 inserted at a decondensed locus will be more compared to when the array is inserted at a condensed
105 locus. This is because, due to condensation, a linear shrinkage of the operators happens which
106 brings the TetR-GFP molecules closer to each other causing quenching of the fluorescence and
107 hence reduction in the intensity (Fig. 1A). The *CEN V*-GFP marked strains also harbored SPBs
108 (Spc42) marked with mCherry to judge different cell cycle stages. The GFP signal intensities were
109 measured in the cells residing at pre-S phase (interphase) stage or at metaphase/metaphase I, which
110 is presumed to contain decondensed and condensed chromatin, respectively. An unbudded cell
111 with a single SPB was taken as a pre-S phase cell in mitosis or meiosis; a large budded cell with
112 two separated SPBs in the mother compartment was taken as a metaphase cell (Fig. 1B) whereas

113 same in an unbudded meiotic cell was considered as a metaphase I cell (Fig. 1C). The timepoint
114 to harvest meiotic pre-S phase cells was determined based on Ime1 (an inducer of meiosis in yeast)
115 expression and FACS analysis. The Ime1 expression is induced by an acetate-based rich medium
116 (YPA), however, it starts accumulating in the nucleus after the depletion of G1 cyclins (Colomina
117 et al., 1999, 2003). In our experimental condition also, Ime1 expression started in YPA followed
118 by its nuclear localization around 30 mins in SPM with no nuclear localization either in YPA or
119 hardly any in SPM at 10 mins (Fig. S1A, B). FACS analysis showed that the DNA synthesis started
120 before the cells were at least 90 mins in SPM (Fig. S1C). Based on these observations, 1 hr into
121 SPM was taken as the timepoint to harvest meiotic pre-S phase cells. For metaphase I cells, the
122 sample was harvested at 6 hrs in SPM, and cells with SPB-SPB distance more than 1 but less than
123 3 μm were analyzed as described before (Tsuchiya et al., 2014, Yu and Koshland, 2005). The
124 mitotic pre-S phase was determined based on Cln2 expression (yeast G1/S-CDK) as its expression
125 marks the beginning of mitosis (Hadwiger et al., 1989) (Fig. S1D).

126 The strategy followed for accurately measuring *CEN V*-GFP signal intensity normalized
127 with internal control (Spc42-mCherry) from four different types of samples – mitotic interphase,
128 metaphase, meiotic interphase, and metaphase I cells is described in materials and methods. As
129 expected, both in mitosis and meiosis, the *CEN V*-GFP fluorescence intensity decreases in the
130 metaphase and metaphase I cells, respectively than in the corresponding interphase cells
131 reconfirming that condensation occurs as the cells enter into the cell cycle (Lavoie et al., 2004;
132 Vas et al., 2007). Interestingly, while in mitosis, the extent of decrease was 30.9% (1.13 vs 0.78
133 A.U., Fig. 1B), the same was 47% (1.33 vs 0.7 A.U., Fig. 1C) in meiosis. The ~1.5-fold decrease
134 in signal intensity in meiosis over mitosis argues for an increased level of chromosome
135 condensation in meiosis than in mitosis. Since *CEN V*-GFP fluorescence intensity was measured
136 from different mitotic and meiotic cells, an error in measuring the intensity across the samples may

137 lead to the observed difference in fluorescence intensity between mitosis and meiosis. To rule out
138 this possibility we mixed the mitotic and meiotic cells and measured the fluorescence intensity
139 from the metaphase or metaphase I cells residing in the same field of view. The metaphase cells
140 with two SPBs and a bud were distinguishable from the metaphase I cells harboring 2 SPBs but
141 no bud. Consistent with the previous observation, we found ~1.7-fold decreases in signal intensity
142 in meiotic metaphase I cells compared to mitotic metaphase cells (0.825 vs. 0.485 A.U., Fig. 1D)
143 indicating chromosomes are indeed more condensed in meiosis than in mitosis.

144

145 **The non-essential kinetochore protein Ctf19 influences chromosome condensation in**
146 **meiosis but not in mitosis**

147 Earlier we and others have reported that the mitotically non-essential kinetochore proteins have
148 essential roles in meiosis (Mehta et al., 2014, Agarwal et al., 2015, Borek et al., 2021). In support
149 of this, we observed that such a protein Ctf19 promotes rDNA condensation in meiosis but not in
150 mitosis (Mehta et al., 2014). Since we revealed that the extent of chromosome condensation, at
151 least at the pericentromeres, is more in meiosis than in mitosis, we wished to investigate the
152 contribution of Ctf19 to this difference. We measured the *CEN V*-GFP signal intensity in the
153 diploid *ctf19Δ* mutant cells from the pre-S phase and metaphase/metaphase I in both mitosis and
154 meiosis. Any meiosis-specific function of Ctf19 on condensation is expected to ameliorate the
155 difference in condensation (or *CEN V*-GFP signal intensity) between the pre-S phase and M phase
156 in meiosis but not in mitosis. We observed a significant (39%) decrease in signal intensity in
157 metaphase cells compared to the pre-S phase cells in the *ctf19Δ* mutant (1.67 vs 1.01 A.U., Fig.
158 2A) like the wild type (Fig. 1B) suggesting that condensation is not compromised in the mutant
159 compared to the wild type in mitosis. In contrast, in meiosis, unlike the wild type which showed a
160 47% decrease in the intensity in meiosis (Fig. 1C), only a ~20% decrease (3.13 vs 2.4 A.U., Fig.

161 2B) was found in the mutant which was not statistically significant indicating that a meiosis-
162 specific chromosome condensation defect occurs in absence of Ctf19. Further, we performed a
163 comparative analysis of condensation status between wild-type and *ctf19*Δ cells across both
164 mitotic and meiotic metaphase stages. We found that the mean intensity value is significantly
165 higher in the mutant in meiosis but not in mitosis, which provides additional validation of our
166 claim that the condensation defect occurs in the mutant, specifically in meiosis (Figure S2) .

167 To examine if the observed condensation defect in the *ctf19*Δ mutant in meiosis is specific
168 to the Ctf19c proteins of the kinetochore, we monitored the *CEN V*-GFP signal in the pre-S phase
169 and metaphase I stage in the cells lacking Slk19, another non-essential protein residing at the
170 kinetochore but not as a component of the Ctf19c (Zeng et al., 1999). We could not observe any
171 chromosome condensation defect in the *slk19*Δ cells as the GFP signal intensity decreased in
172 metaphase I compared to the interphase stage (~50%, 1.12 vs 0.55 A.U., Fig. 2C) as found in the
173 wild type (Fig. 1C). Since we used identical conditions during mitosis and meiosis, the possibility
174 of other factors viz., accessibility of TetR-GFP to the operators or a lower concentration of TetR-
175 GFP responsible for reducing the fluorescence intensity, can be void. Moreover, the control mutant
176 *slk19Δ* behaved as expected.

177 It is possible that the quenching of the fluorophores can happen due to local compaction of
178 the chromatin through nucleosome-nucleosome interaction independent of condensin-mediated
179 condensation function (Kruitwagen et al., 2015, 2018) or the observed difference in fluorescence
180 intensity can be due to differential binding behaviour of TetR-GFP to the [$TetO_n$] array among the
181 strains and the cell cycle stages. Therefore, to correlate the observed condensation defect in the
182 meiotic cells of the kinetochore mutant with condensin-mediated condensation, we used an
183 alternative in-vivo assay to further validate the above observed condensation defect. We evaluated
184 the condensation status in meiosis and mitosis for both the wild type and *ctf19*Δ by using Second

185 Harmonic Generation (SHG) microscopy which relies on generating a second harmonic by the
186 chromatin fibers upon excitation by two-photon microscopy (Yamin et al., 2019, 2022). In this
187 assay, the chromosomes were stained with DAPI and a higher ratio of integrated density to area
188 obtained through the SHG technique corresponds to higher condensation. As expected, we indeed
189 observed an increased condensation in both wild type and *ctf19*Δ in mitotic metaphase as compared
190 to pre-S phase (Fig. S3 A, B). However, when the meiotic cells of the same strains were analyzed,
191 the wild type cells showed significant increase in the ratio of integrated density to area at
192 metaphase I as compared to pre-S phase, but the *ctf19*Δ cells did not show any significant increase
193 in the ratio in meiotic metaphase I (Fig. S3 C, D). These findings further confirm that the *ctf19*Δ
194 cells are indeed compromised in meiotic condensation with no significant effect on mitotic
195 condensation.

196 For further validation, we compared the extent of rDNA condensation using Net1-GFP as
197 the marker as described before (Torres-Rosell et al., 2004, Machín et al, 2005, Mehta et al., 2014)
198 among the wild type, *ctf19*Δ, and *slk19*Δ strains (Fig. 2D). The Net1-GFP signal pattern was
199 visualized in these strains when the cells were arrested at the metaphase I stage (*pCLB2-CDC20*).
200 While around 85% of the wild-type cells showed the 'tight knit' and 'crescent' signal which
201 represent a condensed state of rDNA (Mehta et al., 2014; Kerr et al., 2011), *ctf19*Δ cells showed a
202 reduction (50%) in the frequency and a corresponding increase (50%) in the occurrence of the
203 'puff' signal which corroborates a decondensed state. On the other hand, *slk19*Δ cells showed
204 similar results to the wild type. In mitosis, however, there was no difference in condensation
205 amongst the wild type, *ctf19*Δ, and *slk19*Δ cells (Fig. S4) where the 'line', 'loop', and 'puff'
206 patterns designate condensed, intermediate, and decondensed forms of the rDNA locus,
207 respectively (D'Ambrosio et al., 2008; Dauban et al., 2019). Altogether, from these results, we
208 infer that Ctf19 promotes chromosome condensation in meiosis but not in mitosis and this function

209 appears to be specific for the Ctf19 protein or perhaps for all the non-essential proteins of the
210 Ctf19c of the kinetochore.

211 **Loss of Ctf19 affects axial condensation of the chromosomal arm**

212 The loss of pericentric and rDNA condensation in the *ctf19*Δ mutant prompted us to examine the
213 mutant for linear (axial) condensation of the chromosomal arms which relies on condensin
214 (Kruitwagen et al., 2015). To investigate this, we first wished to test the condensation status of a
215 locus proximal to the telomere V (*TEL V*) as compared to *CEN V*-GFP. For this, we marked
216 chromosomes at two different loci 400 kb away from each other, one was near the *CEN V* (1.4 kb
217 away), as before, and the other one was 21 kb away from *TEL V* using $[TetO]_{224}$–[TetR-GFP] and
218 $[TetO]_{448}$–[TetR-GFP] systems, respectively. Since the number of operators used to visualize *TEL*
219 *V*-GFP was double that of *CEN V*-GFP, the two loci could be visually distinguishable by the
220 brightness of the GFP dots where *TEL* V-GFP appeared much brighter than the *CEN V*-GFP (Fig.
221 3A). The GFP fluorescence intensities were measured from *CEN V* and *TEL V* dots both in the
222 wild type and *ctf19*Δ mutant cells from pre-S phase and metaphase I stages (Fig. 3B-3C). Both
223 *CEN V*-GFP and *TEL V*-GFP dots showed equivalent (*CEN V*= 33.3% decrease; *TEL V*= 25%
224 decrease) and a statistically significant decrease in GFP intensity in metaphase I cells compared to
225 pre-S phase cells in the wild type. The difference in *CEN V*-GFP intensity between here to what
226 has been described in the previous section (33.3% vs 47%) is possibly because of the difference in
227 the intensity of Spc42-mCherry which was used as an internal control for normalization purposes.
228 Nevertheless, in contrast to the wild type, in the *ctf19*Δ mutant the decreases in *CEN V* and *TEL V*
229 intensities in metaphase I cells compared to pre-S phase cells were 15.6% and 12.5%, respectively
230 which were not statistically significant. These results confirm that Ctf19 is important for the
231 condensation of the region proximal to centromeres or telomeres.

232 Next, we wished to examine the axial condensation of the chromosome V arm by
233 measuring the distance between the *CEN V*-GFP (light) and *TEL V*-GFP (bright) dots. In the wild
234 type, we observed a 37% decrease in the mean distance in the metaphase I stage (0.5 µm) compared
235 to the pre-S phase stage (0.8 µm) owing to the condensation (Fig. 3D, left panel). However, in the
236 *ctf19*Δ mutant, there was no significant decrease in the mean distances between the two stages (0.9
237 vs 1.08 µm) suggesting a defect in the condensation (Fig. 3D, right panel). While looking at the
238 axial condensation in mitosis, there was a statistically significant decrease in the distance in
239 metaphase compared to the pre-S phase both in the wild type and the mutant (21% and 24 %,
240 respectively) (Fig. S5). Notably, since the mean distance in the mutant (1.08 µm) was found higher
241 than the wild type (0.8 µm) in the meiotic pre-S phase that precedes condensin function, it is
242 possible that at this phase the compaction of the chromatin is compromised in the mutant due to
243 relaxed nucleosome-nucleosome interaction. Altogether, these results suggest that the contribution
244 of Ctf19 in promoting chromatin condensation in meiosis is not only restricted to the
245 pericentromeric regions but also extends axially along the chromosome arms at the distal loci.

246

247 **Ctf19 is required for maintenance of chromatin-condensin association in meiosis.**

248 Earlier we reported that in absence of Ctf19, the chromatin-condensin association is perturbed in
249 meiosis (Mehta et al., 2014) which supports our findings from the condensation assays described
250 here. We wished to re-verify our earlier observation with further investigation to find whether the
251 effect on chromatin-condensin association is specific to Ctf19c proteins and whether the effect is
252 on the establishment and/or maintenance of the association. To address these, we first compared
253 the localization of the condensin protein Brn1 on the chromatin between the wild type and *ctf19Δ*
254 mutant along with the *slk19Δ* mutant which, as control, showed no effect on condensation (Fig.

255 2C and 2D). Brn1 fused to 6XHA at the C-terminal (Verzijlbergen et al., 2014) was detected on
256 the chromatin in the meiotic cells arrested at metaphase I by Cdc20 depletion. While a similar
257 number (~ 13 to 15) of bright Brn1-6HA foci were visible in the wild type and *slk19Δ* mutant, the
258 number of foci was much lower (~7) and the foci were less bright in the *ctf19Δ* mutant suggesting
259 a defect in chromatin-condensin association in the latter (Fig. S6 A). On the other hand, as expected
260 from the condensation assay results, no difference in Brn1-6HA localization was observed between
261 the wild type and *ctf19*Δ spreads prepared from the cells arrested at mitotic metaphase by Cdc20
262 destruction as mentioned in materials and methods (Fig. S6 B, C). To test if the observed
263 condensation defect is specific to Ctf19 or also occurs in other non-essential proteins of Ctf19c,
264 we analyzed the association of Brn1-6HA with chromatin in cells lacking another protein of
265 Ctf19c, Ctf3. We found that in *ctf3Δ* cells also, the number of Brn1-6HA foci was lesser (~4) than
266 the wild type (~9) (Fig. S7). The lesser number of foci here in the wild type compared to the
267 previous chromatin spread of Brn1-6HA in the wild type (Fig. S6) can be because of technical
268 difference in antibody staining, as these experiments were performed at different times

269 To further validate our chromatin spread data from meiosis, we performed a ChIP assay to
270 quantify the association of Brn1 with different regions of chromosome - centromere,
271 pericentromere, and arm (Fig. 4A). The cells were harvested after 8 and 10 hrs into SPM to obtain
272 metaphase I arrested wild type and *ctf19Δ* mutant, respectively by Cdc20 depletion. We observed
273 a significant reduction in the level of Brn1 at all the regions in the mutant compared to the wild
274 type; however, the reduction was more at the centromeric region compared to other regions (Fig.
275 4B). These results, re-confirming our earlier chromatin spread data (Mehta et al., 2014), further
276 indicate that the meiotic defect in chromatin-condensin association is specific to the lack of Ctf19c
277 proteins.

278 Next, we wished to address whether Ctf19 is required for the establishment or maintenance
279 of chromatin-condensin association. It has been previously shown that during early meiosis,
280 condensin first associates with rDNA as a cluster and then at later time points associates with the
281 rest of the chromatin leaving a minuscule amount at the rDNA (Markowitz et al., 2020; Li et al.,
282 2014). To compare the dynamics of chromatin-condensin association between wild type and
283 *ctf19Δ* we monitored the association of Brn1-6HA with chromatin using chromatin spreads at
284 different time points in the cells released into synchronized meiosis (Fig. 4C). Types 1 – 3 are
285 categorized as localization of Brn1-6HA first at rDNA (type 1) and then gradually spreading to
286 rest of the chromatin (types 2 – 3). Type 4 implies a gross reduction in chromatin-condensin
287 association. While the initial rDNA localization of Brn1-6HA (0 hr, type 1) in the mutant was not
288 found lesser than the wild type, its gross chromatin localization (type 3) in the mutant was merely
289 below 10% of the spreads compared to the wild type (40%) at 4 hrs. This implies that the
290 establishment of condensin association with the gross chromatin, but not with the rDNA, is
291 perturbed in the absence of Ctf19. Consequently, at 8 hrs, while the mutant showed a major
292 population of spreads (70%) with reduced condensin on the chromatin (type 4), only a minor
293 population (<20%) of wild type spreads demonstrated this phenotype. Moreover, as the type1
294 population decreased to 75% in the mutant compared to 50% in the wild type at 6 hrs, this
295 observation may be interpreted as a defect in the maintenance of the rDNA association of
296 condensin in the mutant.

297

298 **The condensation defect in *ctf19*Δ may occur partially through Sgo1 mislocalization but**
299 **independent of DDK- and Ipl1-mediated pathways**

300 Next, we wished to address the mechanism through which Ctf19 may regulate condensation in
301 meiosis. Besides protecting the pericentromeric cohesin in meiosis I, Sgo1 (Shugoshin) has a role

302 in mitotic chromosome condensation (Kruitwagen et al., 2018) through condensin loading at
303 pericentromeric region (Peplowska et al., 2014). It has also been reported that in the absence of
304 Ctf19c proteins, Iml3 and Chl4, the Sgo1 localization becomes compromised at the chromatin both
305 in mitosis (Deng et al., 2018) and meiosis (Kiburz et al., 2005). To investigate if Ctf19, unlike the
306 peripheral Ctf19c components Iml3 and Chl4, differs in recruiting Sgo1 on the chromatin between
307 mitosis and meiosis which may cause the differential effect on condensation, we analyzed the
308 localization of Sgo1-EGFP in mitosis (metaphase) and meiosis (metaphase I) in presence or
309 absence of Ctf19. We observed that the absence of Ctf19 affected Sgo1 localization both in mitosis
310 (Fig. 5A) and meiosis (Fig. 5B), however, the extent of the defect was more in meiosis where 79%
311 of the cells showed Sgo1-EGFP mislocalization (no signal) compared to only 53% in mitosis.
312 Whereas the fraction of cells showing no signal of Sgo1-EGP in the wild type was found similar
313 in mitosis and meiosis (Fig. 5A, B). To further validate our cell biological data, we performed a
314 ChIP assay to quantify the association of Sgo1-9Myc with the centromeres. We observed a
315 significant reduction in the level of Sgo1-9Myc at the centromeres both in mitosis (Fig. 5C) and
316 meiosis (Fig. 5D) in *ctf19*Δ mutant compared to the wild type. However, the reduction was more
317 (~80% for both *CEN III* and *CEN IV*) in meiosis than in mitosis (~ 45% for *CEN III* and ~ 40%
318 for *CEN IV*) (Fig. 5C, D; see materials and methods). Based on these observations, we conclude
319 that a higher reduction in Sgo1's association with the chromatin in meiosis over mitosis in *ctf19*Δ
320 cells may contribute partially, if at all, to the meiosis-specific chromatin-condensin association
321 defect in these cells.

322 It has been reported earlier that till metaphase the rDNA condensation in mitosis is
323 dependent on cohesin (Lavoie *et al*., 2002). As the cohesin loading at the pericentromeres is
324 dependent on Ctf19 through recruitment of DDK (Dbf4-dependent kinase) both in mitosis and
325 meiosis (Hinshaw et al., 2015, 2017), therefore, the reduction of cohesin level at the centromeres

326 in *ctf19*Δ mutant is unlikely the cause for observed meiosis-specific condensation defect. However,
327 recently DDK and Cdc5 (budding yeast polo-like kinase) have been reported to have roles in the
328 meiotic prophase-like pathway (cleavage-independent cohesin removal from the chromatin) which
329 has been shown important for chromosome compaction in meiosis probably by making space on
330 chromatin for condensin loading (Challa et al., 2019). Based on this, we hypothesized that perhaps
331 DDK kinase localization at the centromeres is perturbed in the absence of Ctf19 which in turn
332 results in an impaired prophase-like pathway hence leading to chromosome condensation defect.
333 If our hypothesis is correct, then a DDK mutant unable to be localized at the centromeres should
334 show a condensation defect in meiosis. It has been reported that the fusion of epitopes at the C-
335 terminal of the Dbf4 protein renders it inactive at the centromeres however its localization at the
336 origins of replications remains unaffected (Hinshaw et al., 2017). We constructed a strain
337 expressing Dbf4-9myc with heterozygous tagging of *CEN V* and *TEL V* with GFP. We confirmed
338 that the *DBF4-9MYC* allele is acting as a mutant as we observed a reduced frequency of sister
339 chromatid cohesion (Fig. S8A) as reported earlier (Hinshaw et al., 2015). However, we failed to
340 observe any defect either in axial contraction by measuring the distance between *CEN V* and *TEL*
341 *V* (Fig. S8B) or in condensation of centromeric and telomeric regions measured by fluorescence-
342 based quenching assay (Fig. S8C). Based on these observations we conclude that the absence of
343 DDK at the centromeres in *ctf19Δ* cells is not responsible for the observed condensation defect in
344 these cells in meiosis.

345 Phosphorylation of histone H3 at serine 10 by Aurora kinase B (Ipl1 in budding yeast), has
346 been known to play a crucial role in chromosome compaction both in yeast (Kruitwagen et al.,
347 2015) and mammals (Mora-Bermúdez et al., 2007). Additionally, an in vitro assay has
348 demonstrated an interaction between Ctf19 and Ipl1, which is essential for stabilizing the
349 chromosomal passenger complex (CPC) at the centromeres (Fischböck-Halwachs et al., 2019).

350 However, it is uncertain whether Ctf19 interacts with Ipl1 in vivo and regulates Ipl1's centromeric
351 localization and possibly thereby promotes chromosome condensation in meiosis. To address this
352 question, we performed a ChIP assay to quantify the association of Ipl1 at the centromeres in
353 metaphase I arrested wild-type and *ctf19*Δ mutant cells, harvested at 8 and 10 hours into SPM,
354 respectively. However, our analysis did not reveal any significant reduction in the centromeric
355 enrichment of Ipl1 in the *ctf19Δ* mutant compared to the wild type (Fig. S9). Based on these
356 findings, we conclude that Ctf19 does not regulate Ipl1 localization at the centromeres, at least
357 during meiosis and hence Ctf19's involvement in chromosome condensation is independent of the
358 Ipl1-mediated pathway.

359

360 **Polo-like kinase (Cdc5) level increases in the cells in the absence of Ctf19 in meiosis**

361 Having shown that DDK and Ipl1 kinases are not involved, we wished to identify other factor(s)
362 that may promote meiotic condensation via Ctf19. A kinase switch model for chromosome
363 condensation says that different kinases take turns to regulate the condensation at different stages
364 of the cell cycle (Bazile et al., 2010). For instance, casein kinase II, cyclin-dependent kinase, and
365 polo-like kinase regulate condensation at the interphase, metaphase, and anaphase, respectively.
366 Recently, in budding yeast, the polo-like kinase Cdc5 has been shown to be important for both
367 condensation establishment and maintenance in mitosis (Lamothe et al., 2020). Furthermore,
368 earlier we reported that in meiosis, Ctf19c protein mutants show SPB misduplication and
369 supernumerary SPBs (Agarwal et al., 2015), a phenotype also noticed in meiotic cells
370 overexpressing Cdc5 (Shirk et al., 2011). Therefore, we wished to examine if there is any meiosis-
371 specific misregulation of Cdc5 in the *ctf19*Δ cells which might cause the condensation defect.
372 Surprisingly, we observed a higher level of Cdc5 in the *ctf19*Δ cells in meiosis but not in mitosis
373 when the cells were arrested at metaphase I and metaphase, respectively (Fig. 6A and Fig. S10A).

374 To investigate if the high level is due to increased stability of Cdc5 and/or high expression of the
375 corresponding gene, we first detected the protein level of Cdc5-6HA over time in meiosis after
376 blocking the protein synthesis using cycloheximide (CHX) which was added at 8 hrs and 10 hrs
377 timepoints when the wild type and mutant cells were into SPM medium, respectively. We found
378 that Cdc5 is more stable in the mutant compared to the wild type (Fig. 6B). The difference between
379 the slopes of the lines was significant as calculated using GraphPad Prism 8.0.1 ($p = 0.009$).
380 However, we failed to observe any increased stability of Cdc5 in the mutant in mitosis (Fig. S10B).
381 Moreover, there was no increased expression of the *CDC5* gene observed in the mutant (Fig.
382 S10C). From these results, we conclude that perhaps increased stability and a consequent higher
383 level of Cdc5 in *ctf19*Δ cells in meiosis cause the condensation defect.

384 Despite the high level of Cdc5, its association with chromatin was reduced in *ctf19*Δ mutant
385 compared to the wild type as observed by chromatin spread in meiosis (Fig. 6C). Interestingly,
386 more spreads with reduced Cdc5 (type II in 6C) were found in meiosis compared to mitosis in the
387 mutant (Fig. 6D). The reduction in Cdc5-chromatin association can be possible because of reduced
388 cohesin association with chromatin in the absence of Ctf19 (Mehta et al., 2014, Hinshaw et al.,
389 2017). In the absence of cohesin, the chromatin localization of Cdc5 is compromised and its
390 activity becomes somehow misregulated causing hyper-phosphorylation of condensin subunits
391 leading to condensation defect (Lamothe et al., 2020). Therefore, we hypothesized that the
392 increased level of chromatin unbound Cdc5 in *ctf19*Δ meiotic cells may misregulate the condensin
393 phosphorylation status resulting in a reduced association of condensin with the chromatin with
394 consequent condensation defect (Fig. 4). To test this hypothesis, we monitored the phosphorylation
395 status of the condensin protein Ycg1, as it is an essential subunit for condensin complex
396 recruitment to chromatin (Piazza et al., 2014) and is known to be phosphorylated at multiple sites
397 (St-Pierre et al., 2009). We monitored Ycg1-6HA expression pattern over different time points in

398 cells released synchronously into meiosis till metaphase I arrest (Fig. 7A). At later time points (8
399 hrs and 10 hrs) in SPM, which corresponded to the metaphase I arrested stage, two bands of higher
400 (B1) and lower (B2) mobilities were visible while at early time points (0 and 6 hrs) only one band
401 was visible both in wild type and mutant indicating post-translational modification of Ycg1-6HA
402 as reported earlier (St-Pierre et al., 2009). Since the B1 bands at 6 hrs are of higher intensity
403 compared to the bands at 0 hr, we speculated that 0 and 6 hrs bands harbor unmodified and
404 (unmodified + modified) forms of Ycg1-6HA, respectively. However, it was interesting to note
405 that in the mutant the top band B2 was reproducibly of higher intensity compared to the wild type.
406 We speculated that the B2 band depicts a higher-level modification of Ycg1-6HA and was found
407 more in the mutant compared to the wild type. Treatment of the protein extract from metaphase I
408 arrested cells with lambda phosphatase showed that the modification is phosphorylation (Fig. 7B).
409 A better resolution of the protein bands using Phos-tag gel revealed that B1 band indeed contained
410 unphosphorylated and phosphorylated forms of Ycg1-6HA whereas B2 band harbored hyper-
411 phosphorylated Ycg1-6HA (Fig. 7B). These results suggest that hyper-phosphorylation of
412 condensin protein in the mutant possibly occurs due to excess Cdc5 level in the mutant as observed
413 earlier.

414 It is possible that the hyper-phosphorylated form of Ycg1 in the mutant is less stable which
415 impedes the chromatin-condensin association in the mutant, as observed for Brn1 of the condensin
416 complex (Fig. 4). To verify this, we monitored the Ycg1 level in the CHX chase experiment where
417 the protein synthesis was blocked by adding the drug at 8 hrs and 10 hrs in SPM for the wild type
418 and the mutant, respectively; the samples were harvested at the indicated time points (Fig. 7C).
419 We found that Ycg1 is indeed less stable in the mutant compared to the wild type. The difference
420 between the slopes of the lines depicting the Ycg1 level was also significant as calculated using
421 GraphPad Prism 8.0.1 (p = 0.03). We also tested whether the Ycg1 stability was also impaired in

422 the *ctf19*Δ cells in mitosis. For that, we first arrested both the wild type and *ctf19*Δ cells in
423 metaphase by nocodazole (Fig. S11A) and then added CHX in the media to monitor Ycg1 stability.
424 We found no difference in the Ycg1 stability in the wild type and *ctf19*Δ cells (Fig. S11B, C),
425 indicating that Ctf19 influences the stability specifically in meiosis. From our results, we conclude
426 that higher stability of Cdc5 causes accumulation of the protein in *ctf19*Δ meiotic cells, which
427 results in hyper-phosphorylation of condensin. This hyper-phosphorylated condensin is less stable
428 and possibly why its association with the chromatin decreases (Fig. 4, S12).

429 **Misregulation of Cdc5 influences chromatin-condensin association**

430 If excess Cdc5 is responsible for reduced chromatin-condensin association in *ctf19*Δ meiotic cells,
431 then overexpression of Cdc5 in the wild type cells should emulate that, whereas its depletion
432 should rescue the defect in the mutant. The overexpression of Cdc5 in the wild type was achieved
433 by shuffling the endogenous promoter of *CDC5* with the *CUP1* promoter. We verified the
434 overexpression as a phenotype of metaphase I delay as reported earlier (Shirk et al., 2011, Li et
435 al., 2014) when the cells were treated with 50 μM $CuSO_4$ in SPM against a normal meiotic
436 progression at 10 μm $CuSO_4$ (Fig S13A, B). The cells were released into SPM either in 10 or in
437 50 μm $CuSO_4$ and were harvested at 7 hr (Fig. 8A), since this time point produced maximum
438 number of metaphase I cells while treated with 50 μm $CuSO_4$ (Fig. S13B). In the harvested cells,
439 when we visualized the level of chromatin-condensin association using chromatin spreads, the
440 normal level of Cdc5 (10 μm $CuSO_4$) produced 11 to 13 bright Brn1-6HA foci, while with excess
441 Cdc5 (50 μm $CuSO_4$), the number was much lower (~7) (Fig. 8B, C, S13 C) indicating a defect in
442 the association which is consistent to an earlier report (Li et al., 2014).

443 Next, to examine if the defect in chromatin-condensin association in the *ctf19*Δ meiotic
444 cells can be rescued by depleting Cdc5, we shuffled the *CDC5* promoter with *CUP1* promoter in

445 those cells and followed the above strategy except used 0 μm $CuSO_4$ instead of 50 μm (Fig. 8D).
446 We verified that at 7-8 hrs of SPM release, maximum number of metaphase I cells were present
447 (Fig. S13D, E). With normal level of Cdc5 (10 μm $CuSO_4$), we observed around 6 Brn1-6HA foci,
448 while with no Cdc5 expression (0 μm $CuSO_4$), we could see a significantly higher number of Brn1-
449 6HA foci (~10) (Fig. 8E, F, S13 F) indicating a clear amelioration of the defect. Taken together,
450 the above results suggest that the observed meiosis specific condensation defect in absence of
451 Ctf19 is indeed due to accumulation of Cdc5 in the cells.

452 **Discussion**

453 For the last few decades, the kinetochore-centromere has emerged as a controlling hub for various
454 events of chromosome segregation viz., kinetochore-microtubule attachment, early replication of
455 centromeres, pericentromeric cohesin enrichment, homolog pairing, and chromosome
456 condensation. In budding yeast, the essential kinetochore proteins have been shown to initiate
457 chromosome condensation in *cis* which is believed to extend distal to the centromeres through
458 Sgo1 and a histone deacetylase, Hst2 (Kruitwagen et al., 2018). On the other hand, through a series
459 of studies we and others have demonstrated that the organizational assembly of the kinetochore
460 complex differs between mitosis and meiosis and possibly due to this difference it was found that
461 the mitotically non-essential kinetochore proteins play significant roles in meiosis; consequently,
462 in their absence, meiosis is very poor but not mitosis (Mehta et al., 2014, Aggarwal et al., 2015,
463 Borek et al., 2021). In this work, we surprisingly found that the level of chromosome condensation
464 is more in meiosis than in mitosis and the non-essential kinetochore proteins play a role in the
465 regulation of the meiotic condensation through modulation of polo-like kinase Cdc5.

466

467 **Chromosome condensation: mitosis vs meiosis**

468 Regardless of the mode of the cell cycle, chromosomes need to be condensed as they embark into
469 partitioning. However, there are fundamental differences in how the chromosomes behave as they
470 enter into mitosis or meiosis (meiosis I, in particular). One of the major differences is the pairing
471 of the homolog in meiosis which is believed to start at the centromeres by 'centromere coupling'
472 (Tsubouchi et al., 2005) and proceeds towards the telomeres in a zipper-like fashion. It is obvious
473 that finding the right partners and the completion of lengthwise pairing will be more efficient if
474 the units undergoing pairing are shorter and more condensed. Moreover, the post-pairing events
475 including chiasmata formation and resolution of the chiasmata by 'terminalization' of the cross-
476 over point are also presumably favored by more condensed chromosomes. Notably, in pachytene
477 during meiosis I, the paired homologs are individually visible as thread-like structures by whole
478 chromatin staining using DAPI even in small yeast nuclear spreads. However, although the
479 homologs never pair in mitosis, they never appear as thread-like structures even with half the DAPI
480 intensity of the pachytene spreads. By using two different methods of in vivo condensation assays,
481 we observed that in budding yeast meiotic chromosomes are indeed more condensed than the
482 equivalent mitotic stage chromosomes (Fig. 1, 3D, S5A). However, since we observed a greater
483 decrease in intensity of GFP foci and distance between them, as readout for chromatin's local
484 compaction and global contraction, respectively, in meiosis, both nucleosome-nucleosome
485 interaction and condensin function may culminate into higher meiosis-specific condensation.
486 Evidence of more chromosome condensation in meiosis is available in nature. For instance, in Rye
487 (*Secale cereale*) it is reported that chromosomes are compacted in meiosis by a factor of 1.7 in
488 length and 1.3 in diameter more compared to mitosis (Zoller et al., 2004). Notably, we have also
489 found 1.7 times more condensation in meiosis compared to mitosis by in vivo assay in budding
490 yeast (Fig. 1D) indicating a similar mechanism across eukaryotes might exist to achieve more
491 chromosome condensation in meiosis.

492

493 **Kinetochore proteins controlling chromosome condensation**

494 Chromosome condensation can be divided into two stages viz., establishment and maintenance,
495 which are regulated by kinases. As the cells enter into the cell cycle, the condensin becomes active
496 and condensation is established through CDKs (Kimura et al., 1998, Sutani et al., 1999). After the
497 metaphase to anaphase transition, as the CDK level starts declining, aurora B kinase and polo-like
498 kinases phosphorylate condensin subunits and thus maintain the condensation (Lavoie et al., 2004,
499 Takemoto et al., 2007, St. Pierre et al., 2009, Walters et al., 2014, Kruitwagen et al., 2018). In
500 budding yeast mitosis, the essential inner kinetochore proteins promote condensation at the
501 centromeres/pericentromeres by recruiting Ipl1 (aurora B) and Cdc5 (polo-like) kinases at the
502 centromeres (Lavoie et al., 2004, St. Pierre et al., 2009). In contrast, the outer essential and the
503 inner non-essential kinetochore proteins were found to be dispensable for condensation (Nakazawa
504 et al., 2008, Kruitwagen et al., 2018) possibly because they do not regulate chromatin localization
505 of Ipl1 and Cdc5. However, given our earlier study reporting meiosis specific reduction in
506 chromatin-condensin association in absence of the non-essential kinetochore protein Ctf19 (Mehta
507 et al., 2014), in this study we show that the effect is specific to the lack of Ctf19c proteins and it
508 is the establishment of the association which is compromised.

509 Since our and other studies showed reduced pericentric cohesin enrichment in
510 *ctf19*Δ cells (Mehta et al., 2014, Fernius and Marston 2009), it can be argued that the observed
511 reduction in condensin-chromatin association in *ctf19*Δ meiotic cells is merely due to pericentric
512 cohesin enrichment defect. This can happen provided i) compared to mitosis, in meiosis, the arm
513 cohesin is sufficiently low due to the meiosis-specific prophase-like pathway of cohesin removal
514 (Challa et al., 2019), which becomes aggravated due to simultaneous loss of cohesin from the
515 preicentromeres and ii) the presence of cohesin must promote condensin binding. But we

516 categorically negate the above possibilities because i) half of the arm cohesin still remains after
517 cohesin removal by a prophase-like pathway (Challa et al., 2019) although earlier works failed to
518 detect any significant difference in arm cohesin between mitosis and meiosis (Glynn et al., 2004,
519 Fernius and Marston 2009) and ii) it was shown that cohesin does not influence condensin binding
520 using biochemical and cell biological assays (Lamothe et al., 2020, Lavoie et al., 2002).

521 Condensation distal from the centromeres can be influenced by non-essential kinetochore
522 proteins through Bub1 and DDK kinases mediated recruitment of Sgo1 (Fernius et al., 2007,
523 Peplowska et al., 2014) and cohesin (Lavoie et al., 2004, Natsume et al., 2013, Hinshaw et al.,
524 2015), respectively, at the pericentromeres which is then believed to extend towards the telomeres
525 through functions of Sgo1 and Hst2 (Kruitwagen et al., 2018). Therefore, we tested whether Sgo1's
526 centromeric localization and DDK activity are further down in meiosis in *ctf19*Δ cells to explain
527 meiosis-specific condensation defects in these cells. We failed to see any effect on condensation
528 in DDK-compromised cells (Fig. S8A, B and C). However, a higher reduction of Sgo1 level at the
529 pericentromeres in meiosis than in mitosis in *ctf19Δ* cells (Fig. 5) argued this as a possible cause
530 of meiosis-specific condensation defect in these cells. Additionally, we observed that the
531 centromeric association of Ipl1 kinase remains unaffected in *ctf19Δ* cells, indicating that Ctf19
532 does not play a regulatory role in condensation through the Ipl1-mediated pathway (Fig. S9).
533 Further studies surprisingly revealed that it is the higher accumulation of Cdc5 in the *ctf19*Δ
534 meiotic cells that perturbs chromatin-condensin association as discussed below.
535

536 **Interaction of kinetochore with polo-like kinase**

537 In budding yeast, the polo-like kinase Cdc5 is targeted to the centromeres through interaction with
538 the kinetochore proteins in mitosis (Snead et al., 2007, Mishra et al., 2019). It is also shown that
539 pericentromeric cohesin enriches Cdc5 at the centromeres which in turn promotes cohesin removal

540 (Mishra et al., 2016). Therefore, as *ctf19Δ* cells show reduced pericentric cohesin enrichment
541 (Fernius et al., 2009, Mehta et al., 2014), it is expected that the association of Cdc5 with the
542 chromatin would be less and that is what we observed (Fig. 6C). But more reduction of Cdc5-
543 chromatin association in meiosis than in mitosis (Fig. 6D) may account for a greater effect of
544 pericentric cohesin loss in meiosis in *ctf19*Δ cells. Earlier it was reported that Cdc5 dislodged
545 from the chromatin, due to global cohesin inactivation, hyper-phosphorylates condensin causing
546 their misfolding but the misfolded and non-functional condensin remains associated with the
547 chromatin (Lamothe et al., 2020). We also noticed hyper-phosphorylation of condensin (Fig. 7A,
548 B), but in contrast observed a huge drop in chromatin-condensin-association in the spreads made
549 from *ctf19Δ* cells (Fig. 4, S6A, S12), possibly because the hyper-phosphorylated condensin
550 generated in our conditions is less stable (Fig. 7C). Notably, while Lamothe et al., 2020, could not
551 find the difference in total Cdc5 level between wild type and cohesin-depleted cells, we observed
552 a substantial increase in Cdc5 level in *ctf19Δ* cells compared to the wild type. That might have
553 caused a different type of hyper-phosphorylation of condensin in our cells compared to their
554 conditions, leading to the dissociation of condensin from the chromatin. Therefore, we conclude
555 that in *ctf19Δ* cells, the meiosis-specific altered behavior of Cdc5 is not only due to pericentric
556 cohesin reduction but also due to its higher stability (Fig. 6B). Currently, it is not known that how
557 the loss of Ctf19 leads to a higher stability of Cdc5 in meiosis. Cdc5 has meiosis-specific roles
558 including degradation of Pds1 in meiosis I (Attner et al., 2013), mono-orientation of sister
559 chromatids by regulating the association of Mam1 protein with kinetochores, step-wise cohesin
560 removal (Lee and Amon, 2003) and dissolution of homolog linkage (Yu and Koshland, 2005).
561 Moreover, unlike mitosis, in meiosis, Cdc5 is degraded by APC associated with meiosis-specific
562 co-factor Ama1 (Okaz et al., 2012). Therefore, a meiosis-specific protein-protein interaction
563 involving Cdc5 is expected. In this context, given a difference in the assembly of kinetochore

564 exists between mitosis and meiosis (Mehta et al., 2014, Borek et al., 2021), the loss of Ctf19 and
565 possibly other non-essential proteins of Ctf19c might create a condition that disfavors normal
566 degradation of Cdc5. One possibility is that in the *ctf19*Δ mutant cells the activity of Mnd2, an
567 antagonist to Ama1 (Oelschlaegel et al., 2005), increases as Mnd2 is believed to physically interact
568 with Ctf19 (Wong et al., 2007). It will be interesting to investigate the status of Mnd2 and Ama1
569 in the *ctf19*Δ mutant.

570 Overall, in this work, we reveal that the chromosomes are more condensed during meiosis
571 than in mitosis which has implications for understanding the complex meiotic chromosome
572 behavior in mammals where the gametogenesis is largely asymmetric and mechanistically varies
573 profoundly between the sexes. In animal cells, there is no evidence of kinetochore inactivation
574 affecting chromosome condensation in meiosis. Since we observed that the non-essential proteins
575 affect condensation in meiosis but not in mitosis, it would be intriguing to examine the
576 condensation status in animal meiotic cells harboring mutations in kinetochore. Finally, the
577 interaction between kinetochore integrity and the functionality of polo-like kinase (Plk) can be
578 explored in animal cells as improper polo-like kinase activity has been linked to aneuploidy and
579 different disease states in humans viz., elevated Plk level has been reported in several types of
580 cancers and neurological disorders (Takai et al., 2005, Ackermann et al., 2011, Korns et al., 2022).

581 **Material and methods**

582 **Yeast strains**

583 All the strains utilized in this work were derived from the SK1 background and are mentioned in
584 Table S1. Chromosome V was fluorescently marked near *CEN V* and *TEL V* using $[TetO]_n$ –[TetR-
585 GFP] system in strains expressing TetR-GFP. An array of 224 copies of the TetO sequence was
586 inserted at locus 1.4 kb away from *CEN V* through homologous recombination (Michaelis et al.,

587 1997, Tanaka et al., 2000). Similarly, $[TetO]_{448}$ array was inserted near *TEL V* between *BMH1* and
588 *PDA1* genes (Kumar et al., 2021). To perform gene deletion, promoter shuffling, and C-terminal
589 tagging of proteins, a PCR-based method was used (Wach, 1996, Longtine et al.,1998, Janke et
590 al., 2004). Relevant plasmid-borne cassettes procured from Euroscarf were employed for these
591 techniques. Yeast transformation was performed as described previously (Guldener et al., 1996).

592 The cells were synchronized in the G1 phase in the YPA medium and then released in YPD and
593 SPM for mitotic and meiotic sample collection, respectively. For the mitotic pre-S phase, the cells
594 were harvested at 45 mins post-release in YPD which corresponds with the start of Cln2
595 expression. The cells were identified microscopically by unbudded cells with one SPB focus. For
596 metaphase, the cells were harvested after 1.5 hrs post-release in YPD and distinguished
597 microscopically by large-budded cells with two SPB foci in the mother bud. For meiosis, the cells
598 were harvested at 1 hr and 6 hrs post-release in SPM for pre-S phase and metaphase I cell,
599 respectively.

600

601 **Meiotic synchronization**

602 Meiotic induction was carried out as described elsewhere (Cha et al., 2000). Typically, the diploid
603 strain of interest was streaked onto a YPD plate (1% yeast extract, 2% peptone, 2% dextrose, 2%
604 agar) for a single colony followed by 48 hrs of incubation. A single colony was then inoculated
605 into 5 ml of YPD broth and left to incubate overnight at 30°C for ~15 hrs. Subsequently, cells from
606 the overnight grown culture were transferred to a 50 ml YPA medium (1% yeast extract, 2%
607 peptone, and 1% potassium acetate) at 0.2 OD_{600} and grown till ~1.4-1.6 OD_{600} which took
608 approximately 13-15 hrs. 1 ml of YPA culture was taken, the cells were diluted appropriately and
609 subjected to sonication at 50% amplitude for 3 secs and observed under microscope for G1 arrest.

610 Once over 85% of G1 arrest was achieved, the cells were washed with sterile distilled water and
611 resuspended in 50 ml of sporulation media (SPM; 0.3% potassium acetate and 0.02% raffinose).
612 Meiotic synchronization was performed at 30°C with continuous shaking at 200 RPM. Samples
613 were harvested from the SPM at specified time intervals for further experimentation. For
614 metaphase I arrest, the cells harboring *CDC20* promoter shuffled with mitotic *CLB2* promoter (Lee
615 and Amon, 2003), were harvested at 8 hrs and 10 hrs for wild type and *ctf19*Δ mutant, respectively.

616 **The arrest of yeast strains at mitotic metaphase**

617 *Using the auxin-induced degron system*

618 Mitotic metaphase arrest was achieved by degrading Cdc20 using the AID degron (Auxin-
619 Inducible Degron) system (Nishimura et al., 2009). In cells expressing *OsTIR1* from the *ADH1*
620 promoter, the AID coding sequence was C-terminally fused to *CDC20*. Cells were grown in YPD
621 from 0.2 to 0.5 OD_{600} before auxin (3-Indoleacetic acid, Sigma) was added at 1.5 mM
622 concentration and the culture was incubated for a further 2 hrs at 30ºC. Metaphase arrest was
623 confirmed by DAPI staining (more than 85% large budded cells with undivided DAPI).

624 *Using nocodazole, a microtubule depolymerizing drug*

625 The cells were inoculated in YPD at 0.2 OD_{600} and grown till 0.5-0.6 OD_{600} before nocodazole (20
626 µg/ml, Sigma) was added to the culture which was incubated for a further 2 hrs under shaking
627 conditions at 30ºC. Metaphase arrest was confirmed by DAPI staining.

628 **Fluorescence microscopy**

629 The cells were grown in YPD or SPM medium for mitotic or meiotic culture, respectively. The
630 cells were harvested and fixed with 4% formaldehyde for 5 mins and then washed twice with 0.1
631 M phosphate buffer before imaging. All fluorescence images were acquired with a Zeiss Axio

632 Observer.Z1 (63X objective, NA = 1.40; Carl Zeiss Micro-Imaging Inc.) equipped with Axiocam
633 camera. The images were processed and analyzed using Zeiss Zen 3.1 software. Image J and Imaris
634 (8.0.2) software were used for intensity and distance measurements, respectively. For all the box
635 plots for the intensity and distance measurements, mean values were compared across the samples.

636 **Intensity measurement**

637 For intensity calculation of a fluorescence signal, Z-stacks with maximum intensity were merged.
638 A Region Of Interest (ROI) was drawn around the signal of interest, and the integrated density was
639 determined to get the 'signal intensity'. ROI of the same size was put elsewhere in the nucleus for
640 background signal and integrated density was determined to get the 'background intensity'. Each
641 signal intensity value was normalized with the background and Spc42-mCherry intensity values
642 to get the 'normalized signal intensity' which was used to plot the graphs. For *CEN V*-GFP
643 intensity comparison between pre-S phase cells and metaphase I cells in meiosis, the normalized
644 signal intensity obtained from metaphase I cells was divided by 2 to obtain intensity per *CEN V*-
645 GFP as at this stage two sister centromeres are glued together by cohesin and two sister *CEN V*-
646 GFP dots appeared as a single dot (Fig S14).

647 **Second Harmonic Generation (SHG) microscopy and analysis**

648 The sample preparation for SHG microscopy was followed as mentioned earlier (Yamin et al.,
649 2019; 2022). Briefly, the cells were harvested and fixed in 4% paraformaldehyde for 20 mins at
650 RT; they were washed with 0.1 M phosphate buffer and stained with DAPI (Invitrogen, #D1306)
651 for 20 mins in dark. The cells were subsequently placed on a polylysine coated slide and allowed
652 to adhere to the slide. After washing the immobilized cells with PBS, mounting solution was added
653 and the slide was covered with a coverslip. Cells were then analyzed by a Zeiss LSM780 inverted
654 Confocal Microscope, with multi-photon Chameleon vision II Laser (laser power > 3 W, pulse

655 width and repetition rate at default settings, tuning range 690‑1040 nm); Lambda−PMT−
656 identifying all the wavelength spectrums. The slides were excited by 768 nm and emission was
657 collected at 414-628 nm. The quantification was carried out using ImageJ software as mentioned
658 earlier (Yamin et al., 2019; 2022).

659 **Chromatin spread and the analysis**

660 Chromatin spread was performed by following the protocol mentioned elsewhere (Mehta et al.,
661 2014) with certain modifications. Cells were harvested from the mitotic culture of 1.0 OD_{600} and
662 at the required time point for meiotic culture. The cells were washed once with spheroplasting
663 solution (1.2 M sorbitol in 0.1 M phosphate buffer) and harvested by centrifugation at 3000 RPM
664 for 3 mins. The cells were resuspended in 0.5 ml of spheroplasting solution supplemented with 5
665 µl of β-mercaptoethanol and 12.5 µl of zymolyase 20T (10 mg/ml, MP Biomedicals) and incubated
666 at 30ºC for 1.5 hrs. Once 80-90% of the cells were spheroplasted (by observing under the
667 microscope), the spheroplasting was stopped by adding 1 ml of ice-cold stop solution (0.1 M MES
668 - pH 6.4, 1 mM EDTA, 0.5 mM $MgCl_2$, 1 M Sorbitol). The spheroplasts were centrifuged at 2000
669 RPM for 3 mins at 4 ºC and resuspended gently in 125 µl of ice-cold stop solution. 60 µl of
670 spheroplasted cells were put on acid-washed glass slides followed by the addition of 40 µl of
671 fixative solution (4% paraformaldehyde, 3.4% sucrose, 10 N NaOH) and 80 µl of 1% lipsol (LIP
672 Equipment and services) over it. After gentle mixing 80 µl of fixative solution was again added to
673 the slides. The content on the slides was mixed and spread gently using a pipette tip and kept at
674 room temperature overnight for drying. The slides were then washed with 2 ml of 0.4% photo
675 flow-200 (Kodak) and then submerged in 1X PBS for 15 mins. The excess liquid was removed
676 and 100 µl of blocking solution (10 mg/ml BSA in 1X PBS + 5% Skim milk) was immediately
677 added over the fixed nuclear spreads which were then covered with coverslips and incubated at

678 room temperature in a humid chamber for 20 mins. The coverslips were removed and 100 µl of
679 primary antibody (1:200) was added to each slide and incubated at room temperature for 60 mins.
680 The primary antibody was rinsed off by submerging the slides 3 times in 1X PBS for 5 mins each
681 and 100 µl of secondary antibody (1:200) was added followed by incubating at room temperature
682 for 60 mins. The slides were again washed in the same way followed by incubation with 100 µl of
683 DAPI (1 µg/ml, Invitrogen) for 30 mins. After PBS wash for 5 mins, 100 µl of mounting solution
684 (90% glycerol supplemented with 1 mg/ml p-phenylenediamine) was added over the slides
685 followed by a clean coverslip which was sealed with transparent nail paint. The primary antibodies
686 used: rat anti-HA (3F10, Roche), mouse anti-HA (12CA5, Roche) and rat anti-Tubulin (MCA78G,
687 Serotec). The secondary antibodies used: Rhodamine (TRITC)-conjugated goat anti-Rat (Jackson)
688 and Alexa Fluor 488 conjugated goat anti-Mouse IgG (Jackson).

689 For calculation of the number of fluorescence foci associated with each chromatin spread,
690 all the Z-stacks with the signals were first merged and then the file was exported to Imaris (8.0.2)
691 software. The images were visualized using '3-D view' tool of the software. Subsequently, the
692 'Spot' tool in the algorithm setting of the software was used to mark the different foci present in
693 the chromatin spreads. The background fluorescence was subtracted using an automated
694 'subtraction' tool, and the number of foci visible for each spread was scored.

695

696 **Indirect immunofluorescence**

697 Immunofluorescence was performed, as mentioned previously (Mittal et al., 2020; Shah et al.,
698 2023). Briefly, cells from meiotic culture were harvested at indicated time points and fixed with
699 4% formaldehyde at room temperature (RT) for 15 mins. The fixed cells were washed once with
700 PBS and spheroplasted in spheroplasting solution (1.2 M sorbitol, 0.1 M phosphate buffer pH 7.5),

701 in the presence of Zymolyase 20T (MP Biomedicals, #32092) (10 mg/ml) and 25 mM β-
702 mercaptoethanol or 1 hr at 30°C. The spheroplasts were mounted on a polylysine coated slide. The
703 cells were then flattened by immersing the slide in -20°C methanol for 5 mins and in acetone for
704 30 s. The slides were dried for 1-2 mins before blocking using 5% skim milk solution prepared in
705 dilution buffer (10 mg/ml BSA in PBS). The cells were incubated with appropriate primary and
706 secondary antibodies for 1 hr at RT. Following several washes with PBS, samples were incubated
707 with DAPI (Invitrogen, #D1306) (1 µg/ml) solution for 20 mins in dark. Finally, the glass slides
708 were sealed with coverslips for imaging after spreading the mounting solution (1 mg/ml
709 phenylenediamine in 90% glycerol). The antibodies and their dilutions (in dilution buffer) were
710 mentioned as follows. Primary antibodies rat anti-tubulin (Serotec, MCA78G) at 1:5000.
711 Secondary antibodies: (TRITC)-labeled goat anti-rat (Jackson, #115485166).

712 **ChIP (Chromatin immunoprecipitation)**

713 Chromatin immunoprecipitation was performed as described previously (Makrantoni et al., 2019)
714 with certain modifications. Chromatin was cross-linked with 1% formaldehyde (30 mins for Brn1-
715 6HA, 1 hr for Sgo1-9Myc, 2 hrs for Ipl1-6HA) at 25°C with shaking of the culture at 100 RPM,
716 followed by the addition of glycine at a final concentration of 125 mM to quench the crosslinking.
717 Cells were harvested and washed twice with 10 ml ice-cold TBS buffer and once with 10 ml 1X
718 FA lysis buffer (50 mM Hepes–KOH pH 7.5, 150 mM NaCl, 1 mM EDTA, 1% Triton X-100,
719 0.1% Na-deoxycholate) supplemented with 0.1 % SDS. The cell pellet was resuspended in 500 µl
720 of ice-cold 1X FA lysis buffer supplemented with 0.5% SDS, 1 mM PMSF and 1X PIC (Protease
721 Inhibitor Cocktail, Roche). An equal volume of glass beads was added and cells were lysed in a
722 mini bead beater (BIOSPEC, India) for 9 cycles (1 min ON, 1 min OFF on ice). The lysate was
723 collected in a pre-chilled 1.5 ml eppendorf tube and centrifuged at 16,000 x g for 15 min at 4°C.

724 The supernatant was removed and the pellet was resuspended in 1 ml ice-cold 1X FA lysis buffer
725 supplemented with 0.1% SDS, 1 mM PMSF and PIC. The tubes were again centrifuged at 16,000
726 x g for 15 mins. The supernatant was discarded and the chromatin pellet was resuspended in 300
727 µl ice-cold 1X FA lysis buffer supplemented with 0.1% SDS, 1 mM PMSF and PIC. The chromatin
728 was then sheared to 300-500 bp using a water bath sonicator (Diagenode SA, Picoruptor, BC 100,
729 LAUDA Germany) for 30 cycles of 30 s ON / 30 s OFF at 4°C. The sonicated sample was then
730 centrifuged at 16,000 x g for 15 mins at 4°C. The supernatant was collected to which 1X FA lysis
731 buffer was again added and re-centrifuged at the same settings. 10 µl of the supernatant was stored
732 as input at -20°C (Whole cell extract, WCE) and the rest was divided into 'plus antibody' (+Ab)
733 and 'minus antibody' (-Ab), 600 µl each. Aliquots (+Ab) were incubated with 5 µg antibody [anti-
734 HA (3F10, Roche) or anti-MYC (AB9106, Abcam)] overnight in rotating conditions followed by
735 incubation with 50 µl of 50% Protein A Sepharose-beads (GE Healthcare,17-0780-01) for 2 hrs at
736 4°C in rotating condition. The beads were washed at room temperature twice with 1 ml of IP wash
737 buffer I (1X FA lysis buffer, 0.1%SDS, 275 mM NaCl), twice with 1 ml of IP wash buffer II (1X
738 FA lysis buffer, 0.1%SDS, 500 mM NaCl), once with 1 ml of IP wash buffer III (10 mM Tris pH
739 8.0, 250 mM LiCl, 0.5% NP-40, 0.5% sodium deoxycholate, 1 mM EDTA) and once with 1 ml of
740 1X TE (Tris EDTA). The beads were resuspended in elution buffer (50 mM Tris, pH 8.0, 10 mM
741 EDTA, 1% SDS) and incubated overnight at 65°C for de-crosslinking. De-crosslinked samples
742 were treated with Proteinase K (SRL, India) at 45 °C for 2 hrs followed by P:C:I
743 (Phenol:Chloroform:Isoamyl, Himedia) purification. Purified samples were further used for qPCR
744 analysis using CFX96 Real-Time system (BioRad) and SYBR green dye (BioRad) for detection.
745 Enrichment/Input was calculated by the following equation: $\%\,Encrichment/input =$
746 $E\hat{}(-\Delta \mathrm{Ct})$; where, E is the primer efficiency and was calculated by plotting Ct values of serially
747 diluted input with respect to Log dilution. E = $(-1)/\mathrm{slope}$ and $\Delta Ct = Ct_{(Test\ sample)} - (Ct_{(Input)} - Log$

748 *E (Input dilution factor).* Primers used for PCR amplification are given in Table S2. For calculation
749 of percentage decrease of Sgo1-9Myc enrichment at the centromeres in the ChIP assays (Fig 5C
750 and D) following formulae was used: % decrease = $\frac{WT-MT}{WT} x\ 10$; (WT and MT are average
751 enrichment/input values from the wild type and the mutant, respectively).

752

753 **Protein isolation and western blotting**

754 Samples for western blotting were prepared by resuspending the cells in 200 µl of 20% TCA.
755 Equal volume of glass beads was added, and bead beating was done using a mini bead beater
756 (BIOSPEC, India) for 5 cycles (1 min ON, 1 min OFF on ice). Supernatant was collected by
757 centrifugating at 2800 RPM for 2 mins. 400 µl of 5% TCA was again added to the beads and
758 supernatant was again collected after centrifugation. The total supernatant obtained (600 µl) was
759 centrifuged at maximum speed (13,500 RPM) for 5 mins to precipitate the protein. The supernatant
760 was removed, and the protein pellet was resuspended in Laemmli buffer and loaded on SDS-PAGE
761 after boiling at 95°C for 5 mins for further analysis. For phosphatase assay, protocol mentioned
762 elsewhere (Ontoso et al., 2013) was followed with certain modifications. TCA extract in Laemmli
763 buffer was diluted 10-fold in 1X PMP buffer (NEB, Protein Metallo Phosphatases) supplemented
764 with 1 mM $Mncl_2$. The diluted sample was treated with 2 µl Lambda protein phosphatase (NEB)
765 and incubated in water bath at 30 °C for 4 hrs. As control, a similar diluted extract but without
766 adding phosphatase was incubated at similar conditions. The protein sample was TCA precipitated
767 and resuspended in Laemmli buffer followed by heating at 95°C for 5 mins. Western blotting was
768 performed using standard procedure. The blots were developed using following antibodies: rat
769 anti-tubulin antibody (MCA78G, Serotec,), mouse anti-HA (12CA5 and 3F10, Roche), HRP-
770 conjugated goat anti-mouse IgG (Jackson), HRP-conjugated goat anti-rat (Jackson). For CHX-

771 chase experiments, the percentage of protein remaining at each time point was calculated by taking
772 the protein level at 0 hr as 100%.

773 **RNA isolation**

774 Total RNA was extracted from meiotic cell culture of 1.5-2 OD_{600} (~2.5 x10^7 cells) using TRIzol®
775 reagent and PureLink® RNA mini kit (Ambion Life Technologies™). The cell pellet was re-
776 suspended in TRIzol® and cell lysis was done using DEPC treated sterile 0.5 mm glass beads. The
777 rest of the protocol was followed as instructed by the supplier (PureLink® RNA mini kit). RNA
778 was eluted in DEPC (Sigma Aldrich Chemicals Pvt. Ltd.) treated sterile water. DNase treatment
779 was done at 37°C for 10 mins using RNAse-free DNase I (Thermo Fisher Scientific) in the buffer
780 supplied with the enzyme. The DNase and salts in the buffer were removed by purification using
781 trizol-based layer separation and pure RNA was recovered from the aqueous layer. To ensure the
782 absence of DNA impurity, end-point PCR was performed.

783 **Biological replicates and statistical methods**

784 The quantitative data shown in all the figures were obtained from two or three biological replicates.
785 The N values in the figure legends are the total number of cells analyzed from combined replicates
786 of individual assay. Box plots were generated using OriginPro software (OriginLab). Statistical
787 significance was estimated using two-tailed student's t-test for mean with $p < .05$ considered to be
788 significant.

789

790 **Competing Interest Statement**

791 The authors declare no competing interests

792 **Acknowledgement**

We acknowledge the central instrumentation facility of IIT Bombay. The SKG laboratory is supported by the Science and Engineering Research Board (SERB), Govt. of India (CRG/2020/000444). DT and PA are supported by CSIR fellowships (09/087(0886)/2017- EMR-I), and (09/087(0972)/2019- EMR-I), respectively. AA is supported by JRF fellowship from Department of Biotechnology (DBT), Govt of India (BT/PR43050/BRB/10/1992/2021).

Author contributions: DT, PA and AA performed experiments. DT and SKG designed experiments, analyzed and interpreted the data. DT and SKG wrote the manuscript.

References

Ackermann, S., Goeser, F., Schulte, J.H., Schramm, A., Ehemann, V., Hero, B., Eggert, A., Berthold, F. and Fischer, M., 2011. Polo-like kinase 1 is a therapeutic target in high-risk neuroblastoma. *Clinical Cancer Research*, *17*(4), pp.731-741.

Agarwal, M., Mehta, G. and Ghosh, S.K., 2015. Role of Ctf3 and COMA subcomplexes in meiosis: Implication in maintaining Cse4 at the centromere and numeric spindle poles. *Biochimica et Biophysica Acta (BBA)-Molecular Cell Research*, *1853*(3), pp.671-684.

Attner, M.A., Miller, M.P., Ee, L.S., Elkin, S.K. and Amon, A., 2013. Polo kinase Cdc5 is a central regulator of meiosis I. *Proceedings of the National Academy of Sciences*, *110*(35), pp.14278-14283.

Bazile, F., St-Pierre, J. and D'Amours, D., 2010. Three-step model for condensin activation during mitotic chromosome condensation. *Cell Cycle*, *9*(16), pp.3263-3275.

Borek, W.E., Vincenten, N., Duro, E., Makrantoni, V., Spanos, C., Sarangapani, K.K., de Lima Alves, F., Kelly, D.A., Asbury, C.L., Rappsilber, J. and Marston, A.L., 2021. The proteomic landscape of centromeric chromatin reveals an essential role for the Ctf19CCAN complex in meiotic kinetochore assembly. *Current Biology*, *31*(2), pp.283-296.

Cha, R.S., Weiner, B.M., Keeney, S., Dekker, J. and Kleckner, N., 2000. Progression of meiotic DNA replication is modulated by interchromosomal interaction proteins, negatively by Spo11p and positively by Rec8p. *Genes & development*, *14*(4), pp.493-503.

819 Challa, K., Shinohara, M. and Shinohara, A., 2019. Meiotic prophase-like pathway for cleavage-
820 independent removal of cohesin for chromosome morphogenesis. *Current genetics*, *65*, pp.817-
821 827.

822 Colomina, N., Garí, E., Gallego, C., Herrero, E. and Aldea, M., 1999. G1 cyclins block the Ime1
823 pathway to make mitosis and meiosis incompatible in budding yeast. *The EMBO journal*, *18*(2),
824 pp.320-329.

825 Colomina, N., Liu, Y., Aldea, M. and Garí, E., 2003. TOR regulates the subcellular localization of
826 Ime1, a transcriptional activator of meiotic development in budding yeast. *Molecular and cellular*
827 *biology*, *23*(20), pp.7415-7424.

828 D'Ambrosio, C., Schmidt, C.K., Katou, Y., Kelly, G., Itoh, T., Shirahige, K. and Uhlmann, F.,
829 2008. Identification of cis-acting sites for condensin loading onto budding yeast
830 chromosomes. *Genes & development*, *22*(16), p.2215.

831 Dauban, L., Kamgoué, A., Wang, R., Léger-Silvestre, I., Beckouët, F., Cantaloube, S. and Gadal,
832 O., 2019. Quantification of the dynamic behaviour of ribosomal DNA genes and nucleolus during
833 yeast Saccharomyces cerevisiae cell cycle. *Journal of structural biology*, *208*(2), pp.152-164.

834 Deng, X. and Kuo, M.H., 2018. Tripartite chromatin localization of budding yeast shugoshin
835 involves higher-ordered architecture of mitotic chromosomes. *G3: Genes, Genomes,*
836 *Genetics*, *8*(9), pp.2901-2911.

837 Dong, Q. and Li, F., 2022. Cell cycle control of kinetochore assembly. *Nucleus*, *13*(1), pp.210-
838 222.

839 Dou, Z., Liu, R., Zang, J., Yao, X. and Liu, X., 2023. The function, structure and dynamic
840 organization of centromeres and kinetochores. *JUSTC*, *53*, pp.1-9.

841 Eckert, C.A., Gravdahl, D.J. and Megee, P.C., 2007. The enhancement of pericentromeric cohesin
842 association by conserved kinetochore components promotes high-fidelity chromosome
843 segregation and is sensitive to microtubule-based tension. *Genes & development*, *21*(3), pp.278-
844 291.

845 Fernius, J. and Hardwick, K.G., 2007. Bub1 kinase targets Sgo1 to ensure efficient chromosome
846 biorientation in budding yeast mitosis. *PLoS genetics*, *3*(11), p.e213.

847 Fernius, J. and Marston, A.L., 2009. Establishment of cohesion at the pericentromere by the Ctf19
848 kinetochore subcomplex and the replication fork-associated factor, Csm3. *PLoS genetics*, *5*(9),
849 p.e1000629.

850 Fernius, J., Nerusheva, O.O., Galander, S., de Lima Alves, F., Rappsilber, J. and Marston, A.L.,
851 2013. Cohesin-dependent association of scc2/4 with the centromere initiates pericentromeric
852 cohesion establishment. *Current Biology*, *23*(7), pp.599-606.

853 Fischböck-Halwachs, J., Singh, S., Potocnjak, M., Hagemann, G., Solis-Mezarino, V., Woike, S.,
854 Ghodgaonkar-Steger, M., Weissmann, F., Gallego, L.D., Rojas, J. and Andreani, J., 2019. The
855 COMA complex interacts with Cse4 and positions Sli15/Ipl1 at the budding yeast inner
856 kinetochore. *Elife*, *8*, p.e42879.

857 Ghosh, S.K., Sau, S., Lahiri, S., Lohia, A. and Sinha, P., 2004. The Iml3 protein of the budding
858 yeast is required for the prevention of precocious sister chromatid separation in meiosis I and for
859 sister chromatid disjunction in meiosis II. *Current genetics*, *46*, pp.82-91.

860 Giet, R. and Glover, D.M., 2001. Drosophila aurora B kinase is required for histone H3
861 phosphorylation and condensin recruitment during chromosome condensation and to organize the
862 central spindle during cytokinesis. *The Journal of cell biology*, *152*(4), pp.669-682.

863 Glynn, E.F., Megee, P.C., Yu, H.G., Mistrot, C., Unal, E., Koshland, D.E., DeRisi, J.L. and Gerton,
864 J.L., 2004. Genome-wide mapping of the cohesin complex in the yeast Saccharomyces
865 cerevisiae. *PLoS biology*, *2*(9), p.e259.

866 Guacci, V., Koshland, D. and Strunnikov, A., 1997. A direct link between sister chromatid
867 cohesion and chromosome condensation revealed through the analysis of MCD1 in S.
868 cerevisiae. *Cell*, *91*(1), pp.47-57.

869 Güldener, U., Heck, S., Fiedler, T., Beinhauer, J. and Hegemann, J.H., 1996. A new efficient gene
870 disruption cassette for repeated use in budding yeast. *Nucleic acids research*, *24*(13), pp.2519-
871 2524.

872 Hinshaw, S.M., Makrantoni, V., Harrison, S.C. and Marston, A.L., 2017. The kinetochore receptor
873 for the cohesin loading complex. *Cell*, *171*(1), pp.72-84.

874 Hinshaw, S.M., Makrantoni, V., Kerr, A., Marston, A.L. and Harrison, S.C., 2015. Structural
875 evidence for Scc4-dependent localization of cohesin loading. *Elife*, *4*, p.e06057.

876 Holt, S.V., Vergnolle, M.A., Hussein, D., Wozniak, M.J., Allan, V.J. and Taylor, S.S., 2005.
877 Silencing Cenp-F weakens centromeric cohesion, prevents chromosome alignment and activates
878 the spindle checkpoint. *Journal of cell science*, *118*(20), pp.4889-4900.

879 Jain, N., Janning, P. and Neumann, H., 2021. 14-3-3 Protein Bmh1 triggers short-range
880 compaction of mitotic chromosomes by recruiting sirtuin deacetylase Hst2. *Journal of Biological*
881 *Chemistry*, *296*.

882 Janke, C., Magiera, M.M., Rathfelder, N., Taxis, C., Reber, S., Maekawa, H., Moreno-Borchart,
883 A., Doenges, G., Schwob, E., Schiebel, E. and Knop, M., 2004. A versatile toolbox for PCR-based
884 tagging of yeast genes: new fluorescent proteins, more markers and promoter substitution
885 cassettes. *Yeast*, *21*(11), pp.947-962.

886 Kerr, G.W., Sarkar, S., Tibbles, K.L., Petronczki, M., Millar, J.B. and Arumugam, P., 2011.
887 Meiotic nuclear divisions in budding yeast require PP2ACdc55-mediated antagonism of Net1
888 phosphorylation by Cdk. *Journal of Cell Biology*, *193*(7), pp.1157-1166.

889 Kiburz, B.M., Reynolds, D.B., Megee, P.C., Marston, A.L., Lee, B.H., Lee, T.I., Levine, S.S.,
890 Young, R.A. and Amon, A., 2005. The core centromere and Sgo1 establish a 50-kb cohesin-
891 protected domain around centromeres during meiosis I. *Genes & development*, *19*(24), pp.3017-
892 3030.

893 Kim, S., Meyer, R., Chuong, H. and Dawson, D.S., 2013. Dual mechanisms prevent premature
894 chromosome segregation during meiosis. *Genes & development*, *27*(19), pp.2139-2146.

895 Kimura, K., Hirano, M., Kobayashi, R. and Hirano, T., 1998. Phosphorylation and activation of
896 13 S condensin by Cdc2 in vitro. *Science*, *282*(5388), pp.487-490.

897 Korns, J., Liu, X. and Takiar, V., 2022. A review of Plks: Thinking outside the (polo)
898 box. *Molecular Carcinogenesis*, *61*(2), pp.254-263.

899 Kruitwagen, T., Chymkowitch, P., Denoth-Lippuner, A., Enserink, J. and Barral, Y., 2018.
900 Centromeres license the mitotic condensation of yeast chromosome arms. *Cell*, *175*(3), pp.780-
901 795.

902 Kruitwagen, T., Denoth-Lippuner, A., Wilkins, B.J., Neumann, H. and Barral, Y., 2015. Axial
903 contraction and short-range compaction of chromatin synergistically promote mitotic chromosome
904 condensation. *Elife*, *4*, p.e10396.

905 Kumar, D., Prajapati, H.K., Mahilkar, A., Ma, C.H., Mittal, P., Jayaram, M. and Ghosh, S.K.,
906 2021. The selfish yeast plasmid utilizes the condensin complex and condensed chromatin for
907 faithful partitioning. *PLoS Genetics*, *17*(7), p.e1009660.

908 Lamothe, R., Costantino, L. and Koshland, D.E., 2020. The spatial regulation of condensin activity
909 in chromosome condensation. *Genes & Development*, *34*(11-12), pp.819-831.

910 Lavoie, B.D., Hogan, E. and Koshland, D., 2002. In vivo dissection of the chromosome
911 condensation machinery: reversibility of condensation distinguishes contributions of condensin
912 and cohesin. *The Journal of cell biology*, *156*(5), pp.805-815.

913 Lavoie, B.D., Hogan, E. and Koshland, D., 2004. In vivo requirements for rDNA chromosome
914 condensation reveal two cell-cycle-regulated pathways for mitotic chromosome folding. *Genes &*
915 *development*, *18*(1), pp.76-87.

916 Lee, B.H. and Amon, A., 2003. Role of Polo-like kinase CDC5 in programming meiosis I
917 chromosome segregation. *Science*, *300*(5618), pp.482-486.

918 Leonard, J., Sen, N., Torres, R., Sutani, T., Jarmuz, A., Shirahige, K. and Aragon, L., 2015.
919 Condensin relocalization from centromeres to chromosome arms promotes Top2 recruitment
920 during anaphase. *Cell Reports*, *13*(11), pp.2336-2344.

921 Li, P., Jin, H. and Yu, H.G., 2014. Condensin suppresses recombination and regulates double-
922 strand break processing at the repetitive ribosomal DNA array to ensure proper chromosome
923 segregation during meiosis in budding yeast. *Molecular biology of the cell*, *25*(19), pp.2934-2947.

924 Longtine, M.S., Mckenzie III, A., Demarini, D.J., Shah, N.G., Wach, A., Brachat, A., Philippsen,
925 P. and Pringle, J.R., 1998. Additional modules for versatile and economical PCR-based gene
926 deletion and modification in Saccharomyces cerevisiae. *Yeast*, *14*(10), pp.953-961.

927 Makrantoni, V., Robertson, D. and Marston, A.L., 2019. Analysis of the chromosomal localization
928 of yeast SMC complexes by chromatin immunoprecipitation. *SMC Complexes: Methods and*
929 *Protocols*, pp.119-138.

930 Markowitz, T.E., Heldrich, J. and Hochwagen, A., 2020. DNA break formation induces
931 Scc2/cohesin-dependent recruitment of condensin to meiotic chromosomes. *bioRxiv*, pp.2020-07.

932 Mehta, G., Sanyal, K., Abhishek, S., Rajakumara, E. and Ghosh, S.K., 2022. Minichromosome
933 maintenance proteins in eukaryotic chromosome segregation. *BioEssays*, *44*(1), p.2100218.

934 Mehta, G.D., Agarwal, M. and Ghosh, S.K., 2014. Functional characterization of kinetochore
935 protein, Ctf19 in meiosis I: an implication of differential impact of Ctf19 on the assembly of
936 mitotic and meiotic kinetochores in Saccharomyces cerevisiae. *Molecular microbiology*, *91*(6),
937 pp.1179-1199.

938 Meraldi, P., McAinsh, A.D., Rheinbay, E. and Sorger, P.K., 2006. Phylogenetic and structural
939 analysis of centromeric DNA and kinetochore proteins. *Genome biology*, *7*, pp.1-21.

940 Meyer, R.E., Chuong, H.H., Hild, M., Hansen, C.L., Kinter, M. and Dawson, D.S., 2015.
941 Ipl1/Aurora-B is necessary for kinetochore restructuring in meiosis I in Saccharomyces
942 cerevisiae. *Molecular biology of the cell*, *26*(17), pp.2986-3000.

943 Michaelis, C., Ciosk, R. and Nasmyth, K., 1997. Cohesins: chromosomal proteins that prevent
944 premature separation of sister chromatids. *Cell*, *91*(1), pp.35-45.

945 Mishra, P.K., Ciftci-Yilmaz, S., Reynolds, D., Au, W.C., Boeckmann, L., Dittman, L.E., Jowhar,
946 Z., Pachpor, T., Yeh, E., Baker, R.E. and Hoyt, M.A., 2016. Polo kinase Cdc5 associates with
947 centromeres to facilitate the removal of centromeric cohesin during mitosis. *Molecular Biology of*
948 *the Cell*, *27*(14), pp.2286-2300.

949 Mishra, P.K., Olafsson, G., Boeckmann, L., Westlake, T.J., Jowhar, Z.M., Dittman, L.E., Baker,
950 R.E., D'Amours, D., Thorpe, P.H. and Basrai, M.A., 2019. Cell cycle–dependent association of
951 polo kinase Cdc5 with CENP-A contributes to faithful chromosome segregation in budding
952 yeast. *Molecular Biology of the Cell*, *30*(8), pp.1020-1036.

953 Mora-Bermúdez, F., Gerlich, D. and Ellenberg, J., 2007. Maximal chromosome compaction occurs
954 by axial shortening in anaphase and depends on Aurora kinase. *Nature cell biology*, *9*(7), pp.822-
955 831.

956 Müller, C.A. and Nieduszynski, C.A., 2012. Conservation of replication timing reveals global and
957 local regulation of replication origin activity. *Genome research*, *22*(10), pp.1953-1962.

958 Nakazawa, N., Nakamura, T., Kokubu, A., Ebe, M., Nagao, K. and Yanagida, M., 2008. Dissection
959 of the essential steps for condensin accumulation at kinetochores and rDNAs during fission yeast
960 mitosis. *The Journal of cell biology*, *180*(6), pp.1115-1131.

961 Natsume, T., Müller, C.A., Katou, Y., Retkute, R., Gierliński, M., Araki, H., Blow, J.J., Shirahige,
962 K., Nieduszynski, C.A. and Tanaka, T.U., 2013. Kinetochores coordinate pericentromeric
963 cohesion and early DNA replication by Cdc7-Dbf4 kinase recruitment. *Molecular cell*, *50*(5),
964 pp.661-674.

965 Nishimura, K., Fukagawa, T., Takisawa, H., Kakimoto, T. and Kanemaki, M., 2009. An auxin-
966 based degron system for the rapid depletion of proteins in nonplant cells. *Nature methods*, *6*(12),
967 pp.917-922.

968 Oelschlaegel, T., Schwickart, M., Matos, J., Bogdanova, A., Camasses, A., Havlis, J., Shevchenko,
969 A. and Zachariae, W., 2005. The yeast APC/C subunit Mnd2 prevents premature sister chromatid
970 separation triggered by the meiosis-specific APC/C-Ama1. *Cell*, *120*(6), pp.773-788.

971 Okaz, E., Argüello-Miranda, O., Bogdanova, A., Vinod, P.K., Lipp, J.J., Markova, Z., Zagoriy, I.,
972 Novak, B. and Zachariae, W., 2012. Meiotic prophase requires proteolysis of M phase regulators
973 mediated by the meiosis-specific APC/CAma1. *Cell*, *151*(3), pp.603-618.

974 Ontoso, D., Acosta, I., van Leeuwen, F., Freire, R. and San-Segundo, P.A., 2013. Dot1-dependent
975 histone H3K79 methylation promotes activation of the Mek1 meiotic checkpoint effector kinase
976 by regulating the Hop1 adaptor. *PLoS genetics*, *9*(1), p.e1003262.

977 Peplowska, K., Wallek, A.U. and Storchova, Z., 2014. Sgo1 regulates both condensin and
978 Ipl1/Aurora B to promote chromosome biorientation. *PLoS Genetics*, *10*(6), p.e1004411.

979 Petersen, J. and Hagan, I.M., 2003. S. pombe aurora kinase/survivin is required for chromosome
980 condensation and the spindle checkpoint attachment response. *Current biology*, *13*(7), pp.590-
981 597.

982 Piazza, I., Rutkowska, A., Ori, A., Walczak, M., Metz, J., Pelechano, V., Beck, M. and Haering,
983 C.H., 2014. Association of condensin with chromosomes depends on DNA binding by its HEAT-
984 repeat subunits. *Nature structural & molecular biology*, *21*(6), pp.560-568.

985 Raghuraman, M.K., Winzeler, E.A., Collingwood, D., Hunt, S., Wodicka, L., Conway, A.,
986 Lockhart, D.J., Davis, R.W., Brewer, B.J. and Fangman, W.L., 2001. Replication dynamics of the
987 yeast genome. *science*, *294*(5540), pp.115-121.

988 Schrader, F., 1939. Kinetic regions in chromosomes. *Nature*, *143*(3612), pp.122-122.

989 Shirk, K., Jin, H., Giddings Jr, T.H., Winey, M. and Yu, H.G., 2011. The Aurora kinase Ipl1 is
990 necessary for spindle pole body cohesion during budding yeast meiosis. *Journal of cell*
991 *science*, *124*(17), pp.2891-2896.

992 Snead, J.L., Sullivan, M., Lowery, D.M., Cohen, M.S., Zhang, C., Randle, D.H., Taunton, J.,
993 Yaffe, M.B., Morgan, D.O. and Shokat, K.M., 2007. A coupled chemical-genetic and
994 bioinformatic approach to Polo-like kinase pathway exploration. *Chemistry & biology*, *14*(11),
995 pp.1261-1272.

996 St-Pierre, J., Douziech, M., Bazile, F., Pascariu, M., Bonneil, É., Sauvé, V., Ratsima, H. and
997 D'Amours, D., 2009. Polo kinase regulates mitotic chromosome condensation by hyperactivation
998 of condensin DNA supercoiling activity. *Molecular cell*, *34*(4), pp.416-426.

999 Sutani, T., Yuasa, T., Tomonaga, T., Dohmae, N., Takio, K. and Yanagida, M., 1999. Fission yeast
1000 condensin complex: essential roles of non-SMC subunits for condensation and Cdc2
1001 phosphorylation of Cut3/SMC4. *Genes & development*, *13*(17), pp.2271-2283.

1002 Takai, N., Hamanaka, R., Yoshimatsu, J. and Miyakawa, I., 2005. Polo-like kinases (Plks) and
1003 cancer. *Oncogene*, *24*(2), pp.287-291.

1004 Takemoto, A., Murayama, A., Katano, M., Urano, T., Furukawa, K., Yokoyama, S., Yanagisawa,
1005 J., Hanaoka, F. and Kimura, K., 2007. Analysis of the role of Aurora B on the chromosomal
1006 targeting of condensin I. *Nucleic acids research*, *35*(7), pp.2403-2412.

1007 Tanaka, T., Fuchs, J., Loidl, J. and Nasmyth, K., 2000. Cohesin ensures bipolar attachment of
1008 microtubules to sister centromeres and resists their precocious separation. *Nature cell*
1009 *biology*, *2*(8), pp.492-499.

1010 Tsubouchi, T. and Roeder, G.S., 2005. A synaptonemal complex protein promotes homology-
1011 independent centromere coupling. *Science*, *308*(5723), pp.870-873.

1012 Vas, A.C., Andrews, C.A., Kirkland Matesky, K. and Clarke, D.J., 2007. In vivo analysis of
1013 chromosome condensation in Saccharomyces cerevisiae. *Molecular biology of the cell*, *18*(2),
1014 pp.557-568.

1015 Verzijlbergen, K.F., Nerusheva, O.O., Kelly, D., Kerr, A., Clift, D., de Lima Alves, F., Rappsilber,
1016 J. and Marston, A.L., 2014. Shugoshin biases chromosomes for biorientation through condensin
1017 recruitment to the pericentromere. *Elife*, *3*, p.e01374.

1018 Visintin, C., Tomson, B.N., Rahal, R., Paulson, J., Cohen, M., Taunton, J., Amon, A. and Visintin,
1019 R., 2008. APC/C-Cdh1-mediated degradation of the Polo kinase Cdc5 promotes the return of
1020 Cdc14 into the nucleolus. *Genes & development*, *22*(1), pp.79-90.

1021 Wach, A., 1996. PCR-synthesis of marker cassettes with long flanking homology regions for gene
1022 disruptions in S. cerevisiae. *Yeast*, *12*(3), pp.259-265.

1023 Walters, A.D., May, C.K., Dauster, E.S., Cinquin, B.P., Smith, E.A., Robellet, X., D'Amours, D.,
1024 Larabell, C.A. and Cohen-Fix, O., 2014. The yeast polo kinase Cdc5 regulates the shape of the
1025 mitotic nucleus. *Current Biology*, *24*(23), pp.2861-2867.

1026 Wilkins, B.J., Rall, N.A., Ostwal, Y., Kruitwagen, T., Hiragami-Hamada, K., Winkler, M., Barral,
1027 Y., Fischle, W. and Neumann, H., 2014. A cascade of histone modifications induces chromatin
1028 condensation in mitosis. *Science*, *343*(6166), pp.77-80.

1029 Wong, J., Nakajima, Y., Westermann, S., Shang, C., Kang, J.S., Goodner, C., Houshmand, P.,
1030 Fields, S., Chan, C.S., Drubin, D. and Barnes, G., 2007. A protein interaction map of the mitotic
1031 spindle. *Molecular biology of the cell*, *18*(10), pp.3800-3809.

1032 Yahya, G., Wu, Y., Peplowska, K., Röhrl, J., Soh, Y.M., Bürmann, F., Gruber, S. and Storchova,
1033 Z., 2020. Phospho-regulation of the Shugoshin-Condensin interaction at the centromere in budding
1034 yeast. *PLoS genetics*, *16*(8), p.e1008569.

1035 Yamin, K., Assa, M., Matityahu, A., and Onn, I., 2020. Analyzing chromosome condensation in
1036 yeast by second-harmonic generation microscopy. *Current Genetics, 66*(2), 437–443. doi:
1037 10.1007/s00294-019-01034-1

1038 Yamin, K., Bijlani, S., Berman, J., Soni, A., Shlomai, J., Buragohain, B. M., and Onn, I., 2022.
1039 Fold-change of chromatin condensation in yeast is a conserved property. *Scientific Reports, 12*(1),
1040 17393. doi: 10.1038/s41598-022-22340-8

1041 Yu, H.G. and Koshland, D., 2005. Chromosome morphogenesis: condensin-dependent cohesin
1042 removal during meiosis. *Cell*, *123*(3), pp.397-407.

1043 Zeng, X., Kahana, J.A., Silver, P.A., Morphew, M.K., McIntosh, J.R., Fitch, I.T., Carbon, J. and
1044 Saunders, W.S., 1999. Slk19p is a centromere protein that functions to stabilize mitotic
1045 spindles. *The Journal of cell biology*, *146*(2), pp.415-425.

1046 Zoller, J.F., Herrmann, R.G. and Wanner, G., 2004. Chromosome condensation in mitosis and
1047 meiosis of rye (Secale cereale L.). *Cytogenetic and Genome Research*, *105*(1), pp.134-144.

1048

1049

1050

1051

1052

1053

1054

1055

1056

1057

1058

1059

1060

1061

Figure 1

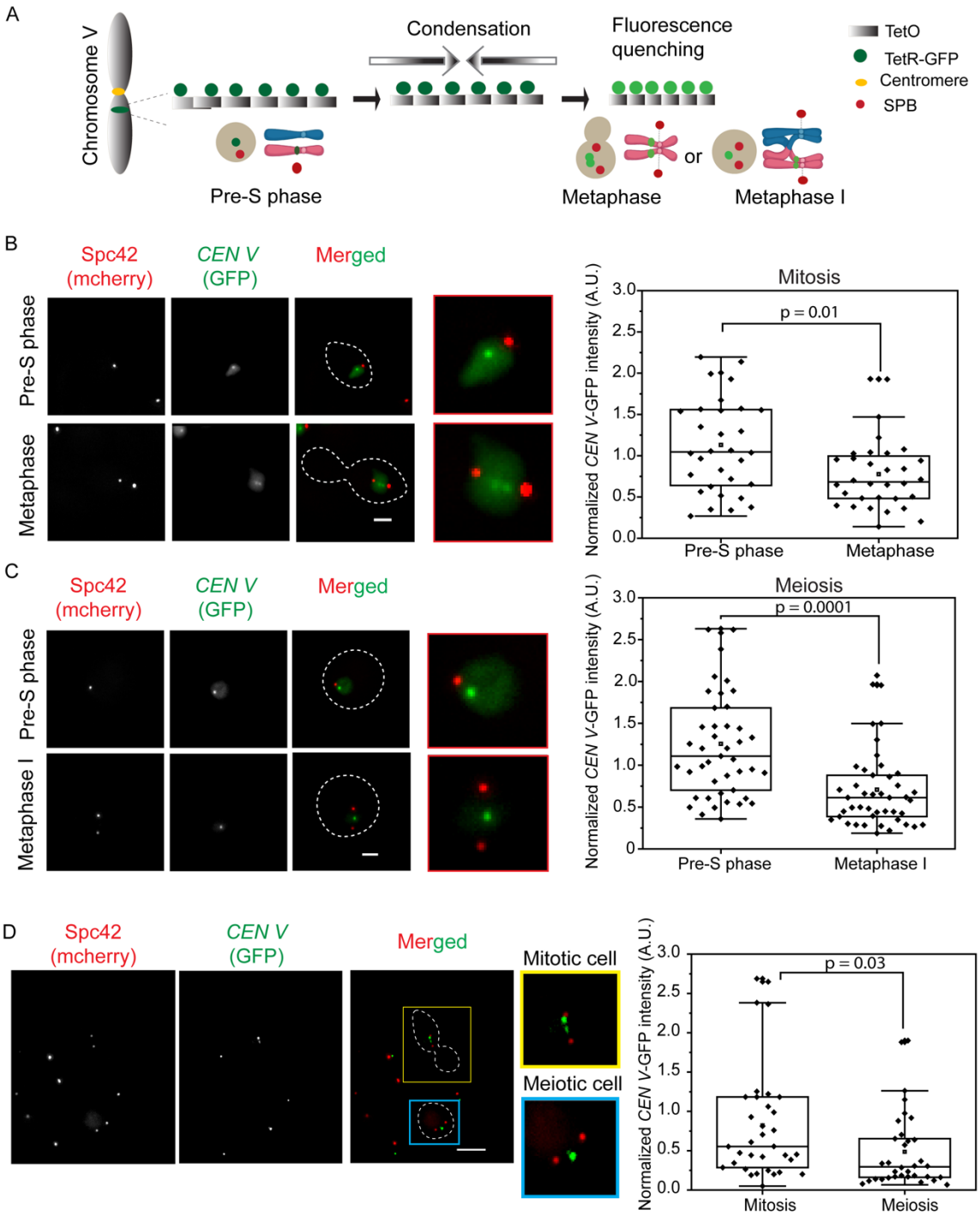

Figure 1. Chromosomes are more condensed in meiosis than in mitosis. (A) Schematic diagrams showing the strategy adopted for in vivo measurement of chromosome condensation. One copy of chromosome V was tagged using $[TetO]_{224}$-[TetR-GFP] system near the centromere V. As the $[TetO]_{224}$ repeats come closer due to axial condensation in the metaphase stage, the GFP signal intensity decreases because of fluorescence quenching. The fluorescence intensity of *CEN V*-GFP measured in (B) mitotic and

1068 (C) meiotic cells (see materials methods for detail) from the indicated cell cycle stages are graphically
1069 represented on the right; the corresponding representative images are shown on the left. N ≥ 30-45 from
1070 three independent experiments, scale bar = 2 µm. (D) The cells used in (B) and (C) were mixed and
1071 fluorescence intensity was measured from mitotic (budded), and meiotic (unbudded) cells present in the
1072 same field of view as represented on the left; the fluorescence intensities are presented graphically on right.
1073 N ≥ 30 from two independent experiments, scale bar = 5 µm. The intensity values were normalized with
1074 background and Spc42-mCherry (internal control) intensities. For statistical significance, *p* values were
1075 estimated by the two-tailed student's t-test for the mean.

Figure 2

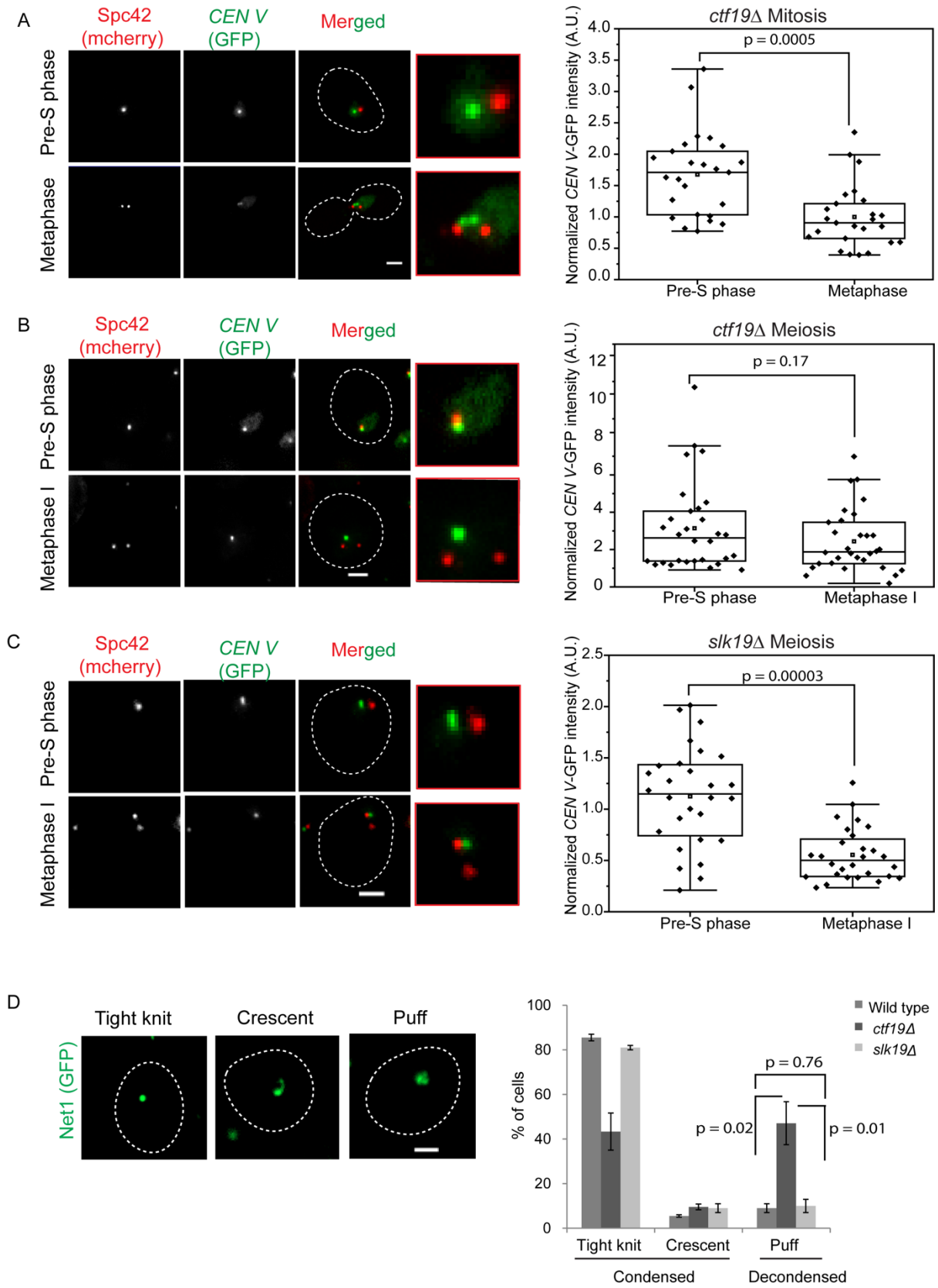

1076

1077 **Figure 2. Ctf19 is involved in chromosome condensation in meiosis but not in mitosis.** In vivo,
1078 chromosome condensation in *ctf19*Δ cells was measured as in Fig. 1 at the indicated stages in mitosis (A)
1079 and in meiosis (B). (C) Similar measurements were done in *slk19*Δ meiotic cells. The intensity values are
1080 graphically represented on the right; the corresponding representative images are shown on the left. N =
1081 25-30 from two independent experiments, scale bar = 2 µm. (D) rDNA condensation in meiosis was
1082 analyzed by visualizing the rDNA-binding protein Net1 tagged with GFP in the wild type, *ctf19*Δ, and
1083 *slk19*Δ cells arrested in the metaphase I stage. N > 200, scale bar = 2 µm. Error bars represent the standard
1084 deviation from the mean values obtained from three independent experiments. For statistical significance,
1085 *p* values were estimated by the two-tailed student's t-test for the mean.

Figure 3

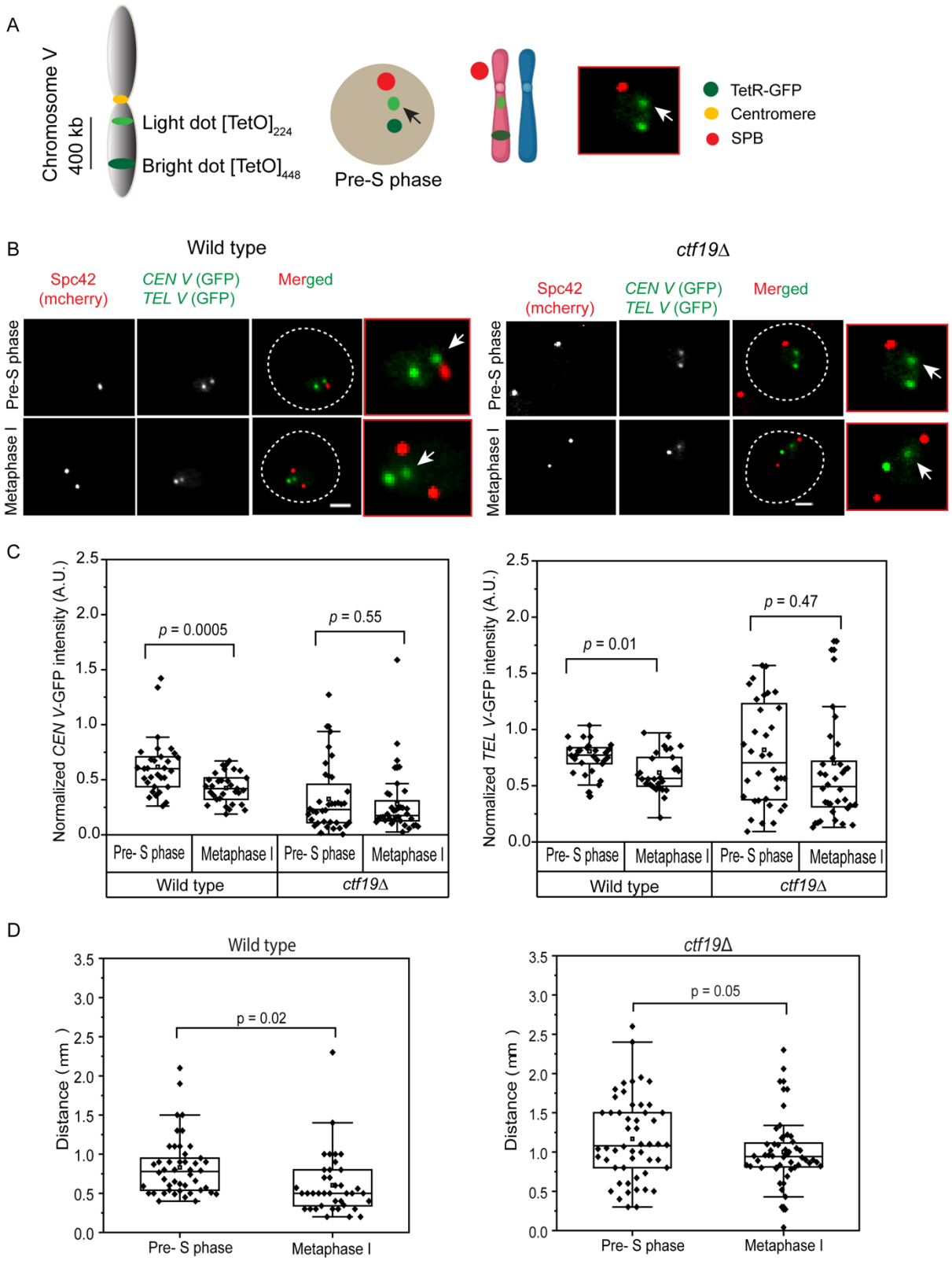

Figure 3. Ctf19 contributes to chromosome condensation along the chromosomal arm (A) One copy of chromosome V was marked with GFP at two different chromosomal loci ~400 kb away from each other,

1089 each proximal to the centromere or telomere was marked with $[TetO]_{224}$–[TetR-GFP] as *CEN V*-GFP or
1090 with $[TetO]_{448}$ –[TetR-GFP] as *TEL V*-GFP, respectively. The *TEL V*-GFP dot appeared brighter than the
1091 *CEN V*-GFP dot (arrow). (B) The representative images are shown for the indicated strains and the cell
1092 cycle stages. Scale bar = 2 µm (C) The *CEN V*-GFP (*left*) and *TEL V*-GFP (*right*) intensities measured as
1093 described in materials and methods are shown for the indicated cells harvested from the indicated cell cycle
1094 stages. N = 25-30 from two independent experiments. (D) The 3D distances between the *CEN V*-GFP and
1095 *TEL V*-GFP dots measured as described in the materials and methods are shown for the wild type (left) and
1096 *ctf19*Δ (right) cells harvested from the indicated cell cycle stages. N = 45-50 from two independent
1097 experiments. The statistical significance *p* value was estimated by the two-tailed student's t-test for the
1098 mean.

1099

Figure 4

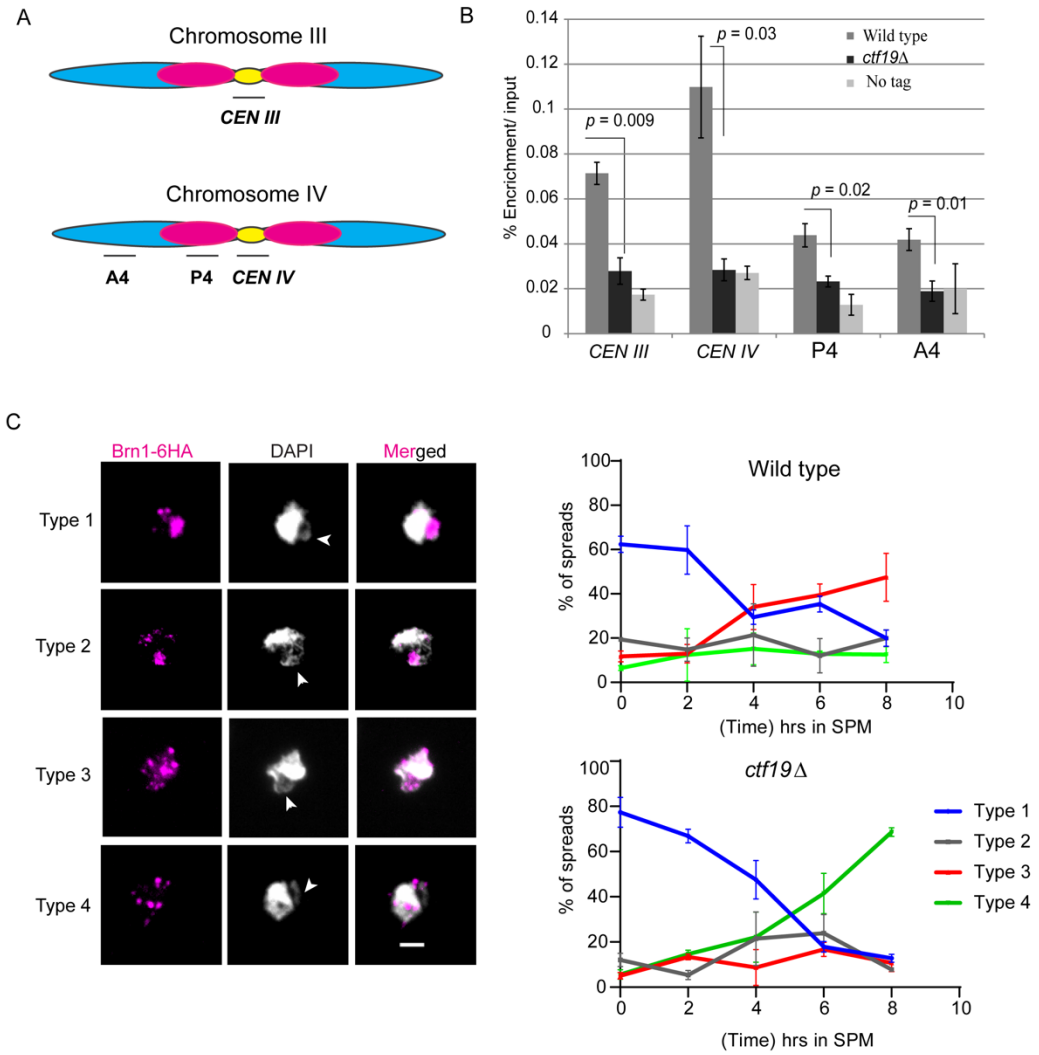

1100

1101 **Figure 4. The loss of Ctf19 causes reduced association of condensin with chromatin by impairing the**
1102 **establishment of the association in meiosis** (A) Schematic diagram showing the locations of PCR
1103 amplicons (horizontal bars) on chromosomes III and IV used for the qPCR analysis of the ChIP samples.
1104 The yellow oval shapes represent the centromeres (*CEN III* and *CEN IV*), pink and blue regions indicate the
1105 pericentromeric (P) and arm (A) regions, respectively. (B) ChIP assay using anti-HA antibodies (3F10) for
1106 quantifying the association of Brn1-6HA with the indicated chromosomal loci in the indicated cells arrested
1107 at metaphase I. The graph represents % enrichment per input obtained by qPCR analysis. Error bars
1108 represent the standard deviation from the mean values obtained from three independent experiments. The
1109 statistical significance *p* value was estimated by the two-tailed student's t-test for the mean. (C) The loss of
1110 Ctf19 impairs the establishment of the association of condensin with chromatin in meiosis. The left panel
1111 shows the representative images of the chromatin spreads showing different types of association (described
1112 in the text) of the condensin subunit (Brn1-6HA) with chromatin at different time points in SPM in wild
1113 type and *ctf19Δ* cells harboring homozygous *BRN1-6HA* allele. Anti-HA antibodies (3F10) were used to
1114 detect Brn1-6HA. The right panel represents the percentage of different types of spreads at the indicated
1115 time points. with respect to the Brn1-6HA signal. Arrowhead shows rDNA region. N >100 from two
1116 independent experiments, scale bar = 2 μm.

Figure 5

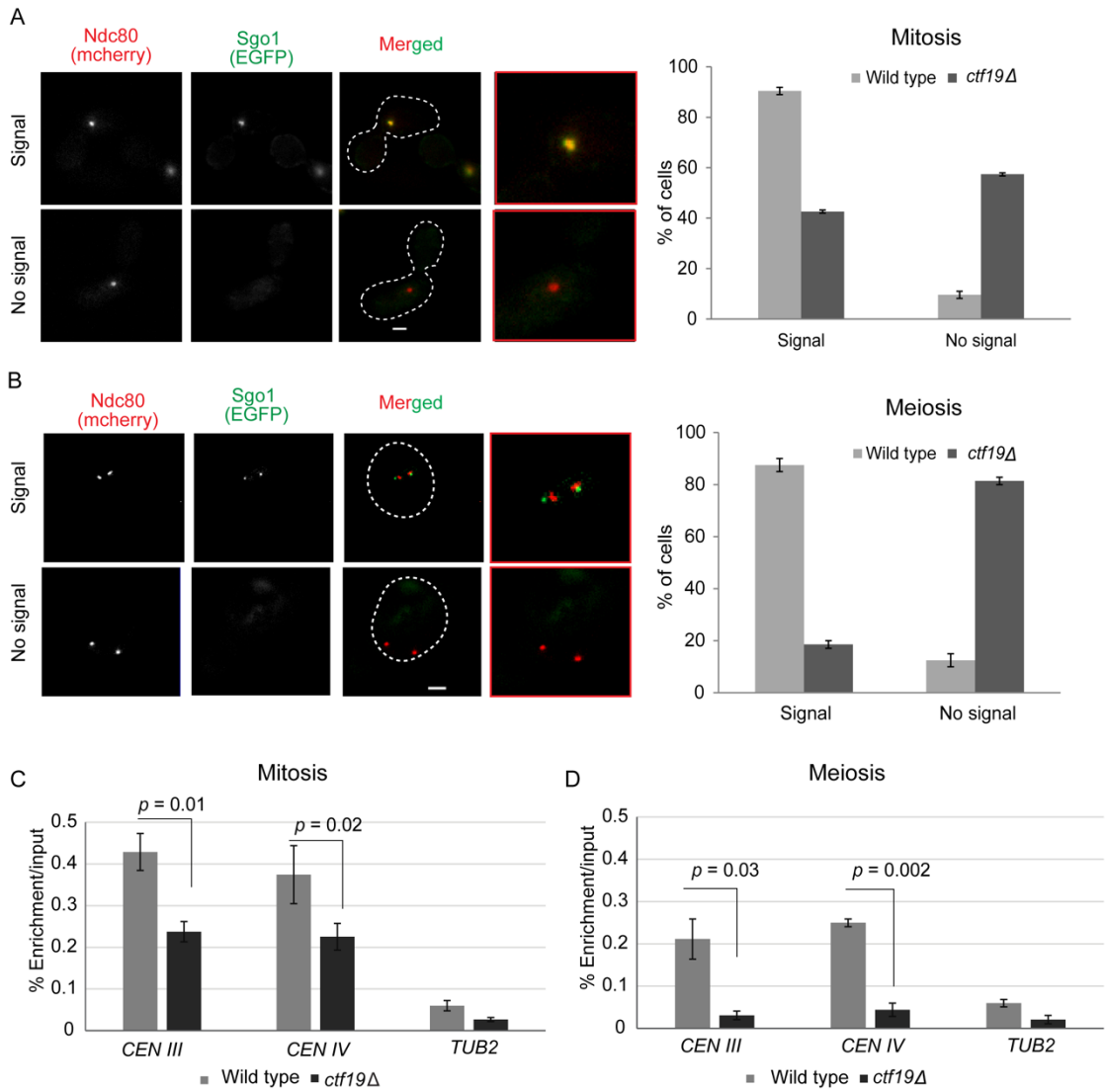

Figure 5. Pericentric localization of Sgo1 is perturbed more in meiosis than in mitosis in the absence of Ctf19. The localization of Sgo1-GFP with respect to a kinetochore protein, Ndc80-mCherry in the wild type and *ctf19*Δ cells arrested at metaphase upon treatment with nocodazole (A) and harvested at metaphase I following their release into SPM for 8 and 10 hrs (B), respectively. The left panel shows the representative images of indicated categories and the right panel depicts the percentage of cells in each category. Error bars represent the standard deviation from the mean values obtained from two independent experiments. N = 90-120, scale bar = 2 µm. ChIP assays using anti-Myc antibodies (ab9106) for quantifying association of Sgo1-9Myc with the indicated chromosomal loci in the wild type and *ctf19Δ* cells arrested at metaphase (C) and metaphase I (D). The graph represents % enrichment per input obtained by qPCR analysis. Error bars represent the standard deviation from the mean values obtained from three independent experiments. The statistical significance *p* value was estimated by the two-tailed student's t-test for the mean.

1129

Figure 6

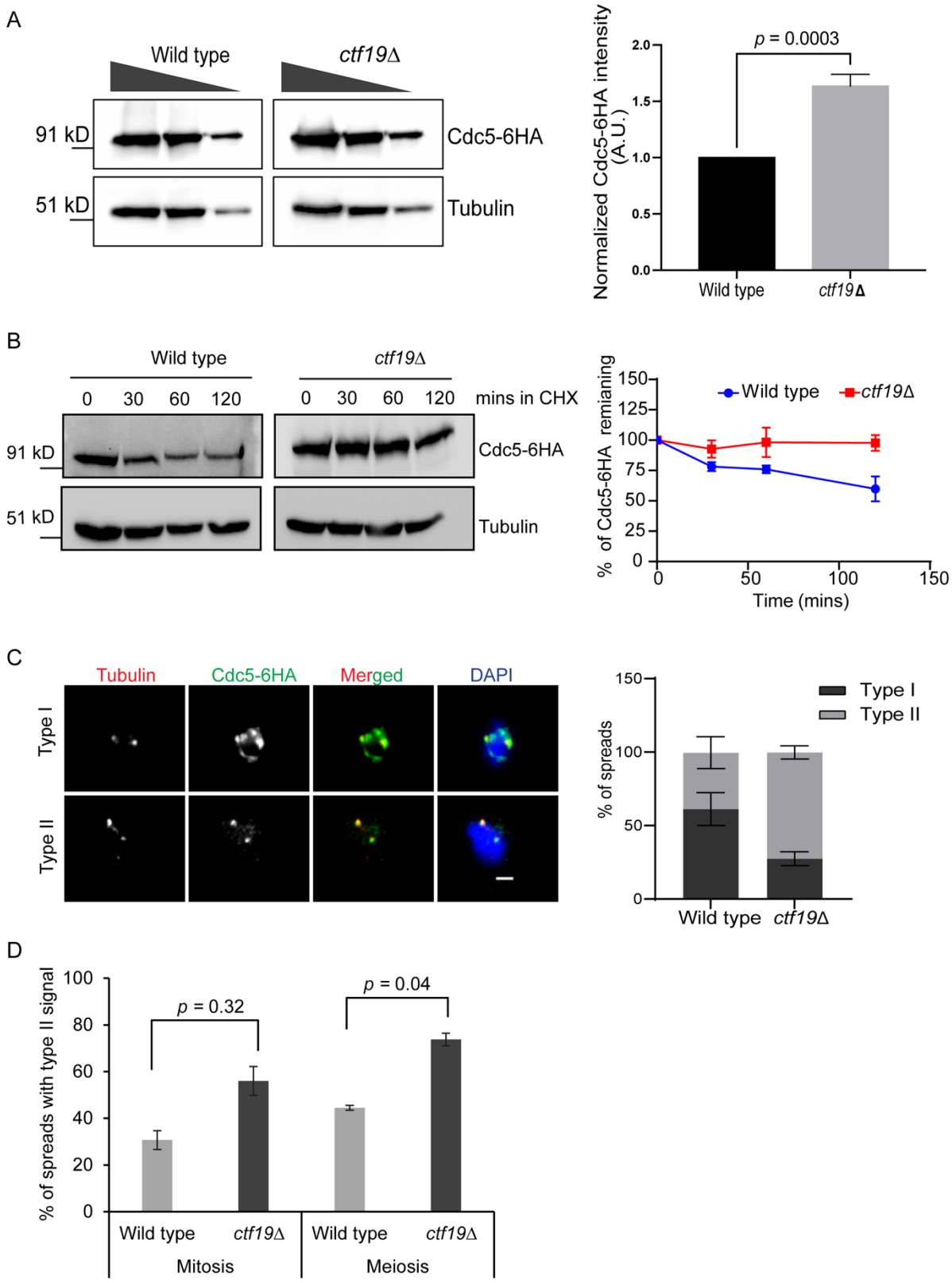

1130

1131 **Figure 6. Increase in the level of Cdc5 and decrease in its chromatin association in *ctf19Δ* mutant in**
1132 **meiosis**. (A) The wild type and *ctf19Δ* cells harboring *CDC5-6HA pCLB2-CDC20* were arrested at the
1133 metaphase I following 8 and 10 hrs of meiotic induction, respectively. Left, the proteins extracted from the
1134 cells were run on a gel in dilutions and were detected by western blotting using anti-HA (3F10) and anti-
1135 tubulin (YOL1/34) antibodies. Right, the intensity of the bands was calculated using ImageJ software and
1136 normalized to the tubulin band intensity used as loading control. *p* value was estimated by the two-tailed
1137 student's t-test for the mean (B) Cdc5-6HA stability in wild type and *ctf19*Δ cells. Following release into
1138 synchronized meiosis for 8 and 10 hrs for the wild type and the mutant, respectively, the cells were treated
1139 with CHX (t = 0). The cells were harvested at indicated time points. Cdc5-6HA and tubulin levels were
1140 analyzed by western blotting (*left*) as in (A) and quantified (*right*) at indicated time points after CHX
1141 treatment. Error bars represent the standard deviation from the mean values obtained from three
1142 independent experiments. (C) Left, the representative images of the chromatin spreads show the association
1143 of Cdc5-6HA with chromatin in metaphase I arrested wild type and *ctf19Δ* cells harboring homozygous
1144 *CDC5-6HA* alleles. Right, quantitative analysis of Cdc5-6HA signal (*right*) on the chromatin spreads as
1145 type I (bright signal) and type II (low signal) categories. The metaphase I stage of the spreads was
1146 determined by SPB localization revealed by tubulin immunostaining. (D) The percentage of chromatin
1147 spreads with type II signal, as mentioned in (C), from the cells arrested in metaphase (mitosis) or metaphase
1148 I (meiosis). Error bars represent the standard deviation from the mean values obtained from two
1149 independent experiments (N = 83, scale bar = 2 μm).

Figure 7

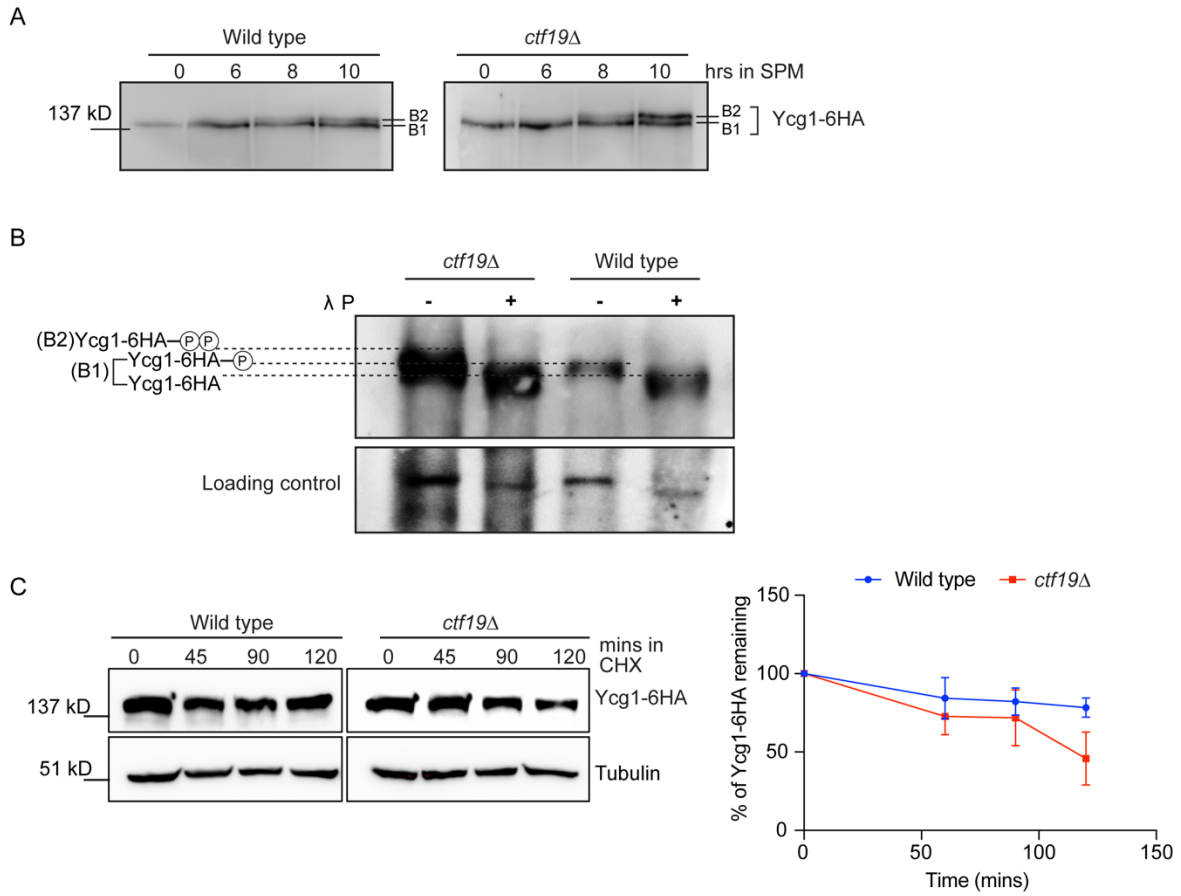

1150

1151 **Figure 7. Evidence of hyper-phosphorylation and reduced stability of Ycg1 in *ctf19* mutant in meiosis**.
1152 (A) The wild type and *ctf19Δ* cells harboring *YCG1-6HA pCLB2-CDC20* were released into synchronized
1153 meiosis and were harvested at the indicated time points; proteins extracted by the TCA method (materials
1154 and methods) from the cells were resolved by running 6% SDS-PAGE gel and were detected by western
1155 blotting using anti-HA antibodies (12CA5). Notably, the B2 band is more prominent than the B1 band in
1156 the mutant. (B) The wild type and *ctf19Δ* cells harboring *YCG1-6HA pCLB2-CDC20* were released into
1157 SPM and the samples were harvested at 8 hrs and 10 hrs, respectively. Protein extracts treated with (+) or
1158 without (-) lambda phosphatase (λ P) were run on 7.5% SDS gel made with Phos-tag acrylamide (Wako)
1159 to detect Ycg1-6HA by western blotting using anti-HA antibodies (12CA5). A non-specific band is shown
1160 as a loading control. (C) Ycg1-6HA stability in wild type and *ctf19*Δ cells. The cells were treated with CHX
1161 (t = 0) following 8 and 10 hrs into meiotic induction for the wild type and *ctf19Δ*, respectively. Left, the
1162 protein extracts were resolved on 10% SDS-PAGE gel and the protein level was analyzed by western
1163 blotting using anti-HA (12CA5) and anti-tubulin (YOL1/34) antibodies in the cells harvested at indicated
1164 time points. Right, quantification of Ycg1-6HA bands normalized with the tubulin bands using ImageJ
1165 software at indicated time points after CHX treatment. Error bars represent the standard deviation from the
1166 mean values obtained from two independent experiments.

1167

Figure 8

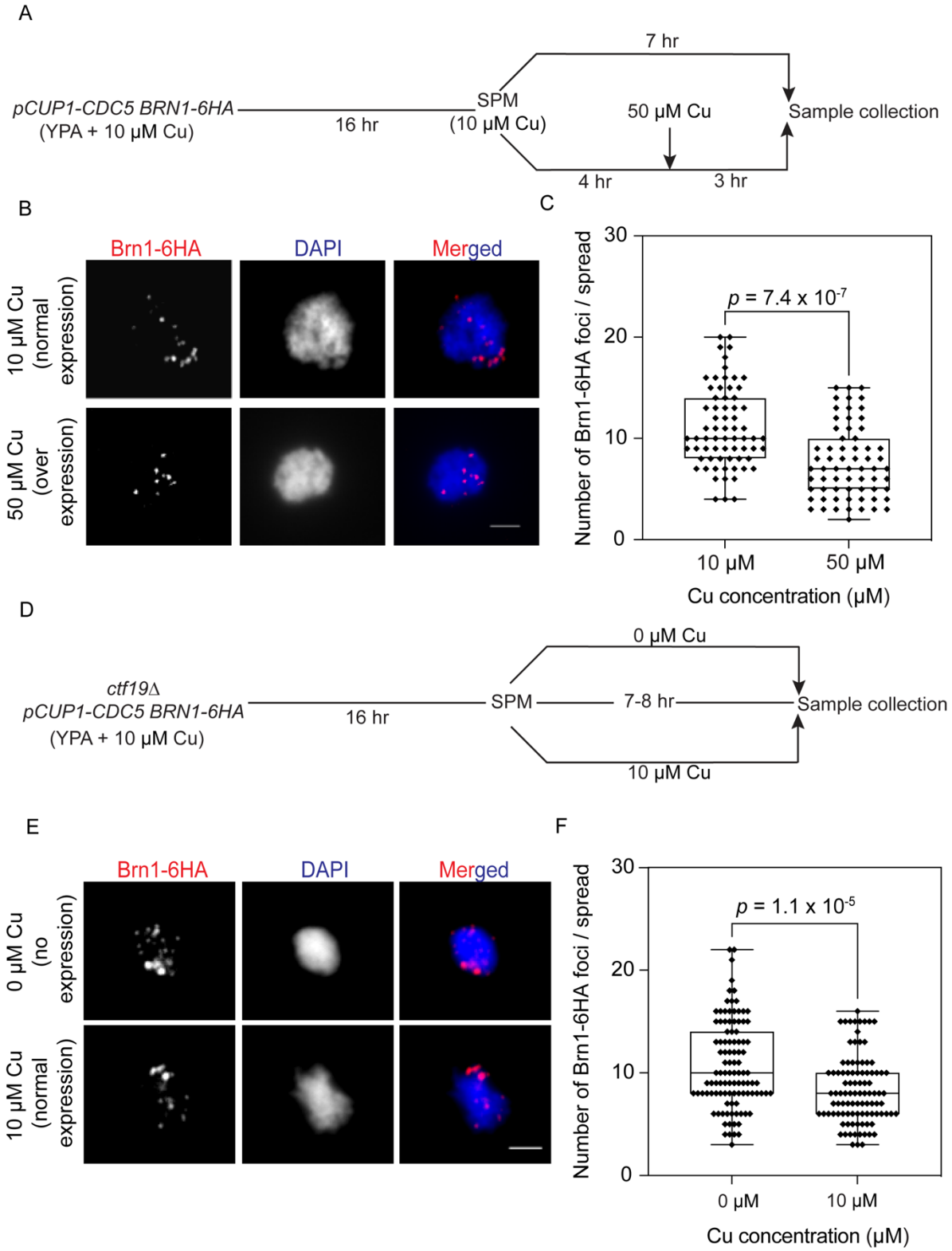

1168

1169 **Figure 8. Misregulation of Cdc5 influences chromatin-condensin association.** (A)
1170 Schematic representation of the experimental strategy. Wild type cells with homozygous *pCUP1-CDC5*
1171 and *BRN1-6HA* alleles were grown in YPA supplemented with 10 μM copper used for normal expression
1172 of *CDC5.* The cells were released into SPM supplemented with either 10 μM or 50 μM (used for over
1173 expression of *CDC5*) copper, respectively. The samples were harvested at the indicated time point for
1174 analysis by chromatin spread assay. (B) Representative images of the chromatin spreads showing
1175 chromatin-Brn1-6HA association under normal or overexpression of *CDC5* in the wild type cells. Anti-HA
1176 antibody (3F10) was used to detect Brn1-6HA. (C) Box plots showing the number of Brn1-6HA foci per
1177 nuclear spread of the wild type cells. N = 60 from two independent experiments. (D, E, F) Same as in A, B
1178 and C, respectively except *ctf19*Δ cells and 0 μM copper was used instead of wild type cells and 50 μM
1179 copper, respectively. For F, N = 80 from two independent experiments. Scale bar = 2 μM. The statistical
1180 significance *p* value was estimated by the two-tailed student's t-test for the mean.

1181

1182